


Cellular/Molecular

Calcium-Dependent Regulation of Neuronal Excitability Is Rescued in Fragile X Syndrome by a Tat-Conjugated N-Terminal Fragment of FMRP

Xiaoqin Zhan,^{1,2}  Hadhimulya Asmara,^{1,2} Paul Pfaffinger,³ and Ray W. Turner^{1,2,4}

¹Hotchkiss Brain Institute, ²Alberta Children's Hospital Research Institute, ³Department of Neuroscience, Baylor College of Medicine, Houston, Texas 77030, and ⁴Department Clinical Neurosciences, University of Calgary, Calgary, Alberta T2N 4N1, Canada

Fragile X syndrome (FXS) arises from the loss of fragile X messenger ribonucleoprotein (FMRP) needed for normal neuronal excitability and circuit functions. Recent work revealed that FMRP contributes to mossy fiber long-term potentiation by adjusting the Kv4 A-type current availability through interactions with a Cav3-Kv4 ion channel complex, yet the mechanism has not yet been defined. In this study using wild-type and *Fmr1* knock-out (KO) tsA-201 cells and cerebellar sections from male *Fmr1* KO mice, we show that FMRP associates with all subunits of the Cav3.1-Kv4.3-KCHIP3 complex and is critical to enabling calcium-dependent shifts in Kv4.3 inactivation to modulate the A-type current. Specifically, upon depolarization Cav3 calcium influx activates dual-specific phosphatase 1/6 (DUSP1/6) to deactivate ERK1/2 (ERK) and lower phosphorylation of Kv4.3, a signaling pathway that does not function in *Fmr1* KO cells. In *Fmr1* KO mouse tissue slices, cerebellar granule cells exhibit a hyperexcitable response to membrane depolarizations. Either incubating *Fmr1* KO cells or in vivo administration of a tat-conjugated FMRP N-terminus fragment (FMRP-N-tat) rescued Cav3-Kv4 function and granule cell excitability, with a decrease in the level of DUSP6. Together these data reveal a Cav3-activated DUSP signaling pathway critical to the function of a FMRP-Cav3-Kv4 complex that is misregulated in *Fmr1* KO conditions. Moreover, FMRP-N-tat restores function of this complex to rescue calcium-dependent control of neuronal excitability as a potential therapeutic approach to alleviating the symptoms of FXS.

Key words: Cav3-Kv4; cerebellum; DUSP; ERK; fragile X syndrome; granule cell

Significance Statement

Changes in neuronal excitability and ion channel functions have been a focus in studies of fragile X syndrome (FXS). Previous work identified fragile X messenger ribonucleoprotein (FMRP) regulates ion channel through either protein translation or direct protein–protein interactions. The current study reveals FMRP is required for the function of a Cav3-Kv4 complex by affecting a Cav3-DUSP-ERK signaling pathway to increase A-type current. In *Fmr1* knock-out cells, calcium-dependent modulation of the A-type current is lost, leading to hyperexcitability of cerebellar granule cells. Pretreating with FMRP-N-tat restores the Cav3-Kv4 function and granule cell excitability, supporting FMRP-N-tat as a potential therapeutic for FXS.

Received Jan. 18, 2024; revised April 4, 2024; accepted April 12, 2024.

Author contributions: X.Z. and R.W.T. designed research; X.Z. and H.A. performed research; P.P. contributed unpublished reagents/analytic tools; X.Z. and R.W.T. analyzed data; X.Z. wrote the paper.

This work was supported by the Canadian Institutes of Health Research and Fragile X Foundation of Canada/FRAXA and a Simons Foundation Autism Research Initiative Explorer Grant. Postdoctoral fellowships (X.Z.) were provided by Fragile X Foundation of Canada/FRAXA (X.Z.), the Hotchkiss Brain Institute, and the Cumming School of Medicine. We gratefully acknowledge J. Forden, F. Visser, and Y. Yu for their expert technical assistance and Dr. N. Cheng for the comments on the manuscript.

The authors declare no competing financial interests.

Correspondence should be addressed to Ray W. Turner at rwtturner@ucalgary.ca.

<https://doi.org/10.1523/JNEUROSCI.0136-24.2024>

Copyright © 2024 the authors

Introduction

Fragile X syndrome (FXS) arises through a CGG repeat expansion in the *Fmr1* gene that blocks the expression of fragile X messenger ribonucleoprotein (FMRP), representing the leading monogenic cause of autism spectrum disorders (ASD). Cell and circuit function in FXS is disrupted because FMRP exerts vast influence over protein translation and modulation of ion channels that control neuronal excitability (Contractor et al., 2015; Deng and Klyachko, 2021). The cerebellum acts as an important sensorimotor interface that impacts the activity

of cortical systems that contribute to ASD (Gallagher and Hallahan, 2012; D’Mello and Stoodley, 2015; Liu et al., 2021; Gibson et al., 2023). A prominent layer of granule cells receive a massive array of mossy fiber input carrying sensory information that is processed to enable time coding, sensorimotor integration, and predictive expectation (D’Angelo and De Zeeuw, 2009; Garrido et al., 2013; Giovannucci et al., 2017; Sgritta et al., 2017; Wagner et al., 2017). Control over the excitability of granule cells could then exert significant influence on higher levels of circuit function relevant to ASD and FXS.

Membrane excitability in granule cells is known to be highly sensitive to the availability of Kv4 potassium channel-mediated “A-type” current (I_A). Bursts of mossy fiber input to granule cells were shown to reduce I_A through a mechanism that involves ERK1/2 (ERK), a kinase increasingly recognized for its role in FXS and ASD (Curia et al., 2013; Osterweil et al., 2013; Asiminas et al., 2019; Murari et al., 2023). A resulting increase in the rate of spike firing then contributes to long-term potentiation (LTP) of mossy fiber input (Zhan et al., 2020). Cerebellar granule cells also express a Cav3-Kv4 complex that invokes calcium-dependent modulation of Kv4 availability through association with a calcium-sensing KChIP3 protein (Anderson et al., 2010a; Heath et al., 2014; Vierra and Trimmer, 2022). Recently FMRP was found to be closely associated with the Cav3-Kv4 complex (Zhan et al., 2020), yet the manner in which FMRP integrates into the complex and how ERK is involved in controlling I_A and membrane excitability is unknown.

The current study reveals a novel signaling pathway whereby Cav3.1 calcium influx activates the phosphatase DUSP1/6 to reduce activated ERK and phosphorylation of subunits in the complex that increases I_A availability. FMRP proves to be critical to the calcium-dependent modulation of Kv4.3 as well as the expression levels of DUSP6, where the loss of FMRP in *Fmr1* knock-out (KO) mice leads to hyperexcitability in cerebellar granule cells. Yet all aspects of Cav3-Kv4 complex function and granule cell excitability are rescued in *Fmr1* KO cells within 24 h of reintroducing a tat-conjugated N-terminal fragment of FMRP. The results thus identify a new signaling pathway that depends on FMRP to control the influence of IA on intrinsic excitability of a key cell type in receipt of sensory input.

Materials and Methods

Cell lines

tsA-201 cells originally derived from a female were purchased from Sigma-Aldrich (catalog #96121229) and maintained in DMEM supplemented with 10% heat-inactivated fetal bovine serum and 1% penicillin-streptomycin at 37°C (5% CO₂). The calcium phosphate method was used to transiently transfect cDNAs of heterologous proteins. Cells were washed with fresh medium 16–18 h after transfection and then transferred to 32°C (5% CO₂) and cultured for up to 36 h prior to tests. Previous work has determined that tsA-201 cells we use do not endogenously express Cav3.1 or Kv4 channels (X. Zhan, unpublished observations) and have no expression of KChIP3 (Extended Data Fig. 1-1). For different experiments, cells were transfected with different combinations of human cDNA Cav3.1 (2.2 µg), Kv4.3 (1.5 µg), and KChIP3 cDNA (1.5 µg) as indicated in Results and figures. In addition, cells were transfected with eGFP cDNA (1 µg) and human Kir2.1 cDNA (1 µg) for electrophysiology and high potassium stimulation experiments, respectively. CRISPR-Cas9 was used to create an *Fmr1* KO tsA-201 cell line (Extended Data Fig. 1-2). For this three short-guide oligonucleotides were synthesized, annealed, and cloned into the pSpCas9(BB)-2A-GFP (pX458) vector (Addgene), and constructs were then transfected into tsA201 cells with Lipofectamine 2000 (Invitrogen). After transfection, GFP containing cells were sorted into 96-well plates by flow cytometry. Western

blotting and DNA sequencing were used to confirm functional KO of the *Fmr1* gene. All *Fmr1* KO tsA-201 cells used in the experiments were maintained from clone 7. To verify that KO of *Fmr1* did not alter subunit expression, we conducted a Western blot on cells coexpressing Cav3.1-Kv4.3-KChIP3 and found no significant difference for any of the subunits between wild-type (WT) and KO cells (Extended Data Fig. 1-3).

Mouse lines

WT (Jackson Laboratory stock #004828, FVB.129P2-Pde6b + Tyrc-ch/AntJ, <https://www.jax.org/strain/004828>) and *Fmr1* KO (Jackson Laboratory stock #004624, FVB.129P2-Pde6b + Tyrc-ch *Fmr1tm1Cgr/J*, <https://www.jax.org/strain/004624>) mice were maintained in Animal Resource Center of the University of Calgary in accordance with guidelines of the Canadian Council of Animal Care. Animals had *ad libitum* access to water and food with a temperature of 20–23°C on a 12 h light and dark cycle.

Cerebellar slice preparation

Sagittal cerebellar sections of 250 µm thickness were prepared from postnatal day 21 (P21) to P25 male mice as previously described (Anderson et al., 2010a). Briefly, after isoflurane inhalation anesthesia, animals were decapitated, and the cerebella were dissected out and placed in ice-cold artificial cerebrospinal fluid (aCSF) composed of the following (in mM): 125 NaCl, 25 NaHCO₃, 25 D-glucose, 3.25 KCl, 1.5 CaCl₂, and 1.5 MgCl₂ bubbled with carbogen (95% O₂ and 5% CO₂) gas. Tissue slices were cut by a vibratome (Leica VT1200 S) and recovered for 20–30 min at 37°C before storing at room temperature (25°C) in carbogen-bubbled aCSF before the transferral to a recording chamber on the stage of an Olympus BX51W1 microscope maintained at 32°C. Whole-cell recordings were obtained in granule cells of lobule 9.

Electrophysiology

Whole-cell patch recordings were obtained using a MultiClamp 700B amplifier and Digidata 1440A to digitize at 40 kHz and analyzed with pClamp 10.5 software. Glass pipettes of 1.5 mm OD (A-M Systems) were pulled using a P-95 puller (Sutter Instruments; 4–8 MΩ). For voltage clamp recordings, series resistance was compensated to at least 70%, and the leak was subtracted off-line in pClamp software. Kv4 activation and inactivation plots were recorded from a holding potential of –110 mV stepped in 10 mV (1,000 ms) increments to 60 mV, followed by a return step to –30 mV (500 ms) as the test potential. Inactivation curves were fitted according to the Boltzmann equation, $I/(I - I_{max}) = 1/[1 + \exp((V_h - V)/k)]$, where V_h is the half inactivation potential and k is the slope factor. Activation curves were fitted by the Boltzmann equation, $G/(G - G_{max}) = 1/[1 + \exp((V_a - V)/k)]$, where G is calculated with $G = I/(V - V_{rev})$. V_a is the half activation potential and k is the slope factor. Inactivation and activation plots were constructed using Origin 8.0 (OriginLab).

tsA-201 cells. Recordings of Kv4.3 current expressed in tsA-201 cells that express FMRP (WT) or in which *Fmr1* was knocked out by CRISPR-Cas9 (KO; Extended Data Figs. 1-2, 1-3) were carried out at room temperature with an external solution (pH adjusted to 7.3 with NaOH) composed of the following (in mM): 125 NaCl, 3.25 KCl, 1.5 CaCl₂, 1.5 MgCl₂, 10 HEPES, 10 D-glucose, and 2 TEA. Pipettes were filled with a solution composed of the following (pH 7.3 with KOH; in mM): 110 potassium gluconate, 30 KCl, 1 EGTA, 5 HEPES, and 0.5 MgCl₂, with 5 di-tris-creatine phosphate, 2 Tris-ATP, and 0.5 Na-GTP added from fresh frozen stock each day. Where indicated, internal levels of calcium concentration were adjusted according to the MaxChelator calculations. Previous work (Turner et al., 2016) and unpublished tests on the effects of exchanging internal electrolyte with drugs or a buffered calcium concentration assure complete exchange of the effective internal levels of calcium in 5–10 min of breaking into the whole-cell recording mode.

Cerebellar granule cells. Current clamp recordings of granule cells from cerebellar sections used an internal solution modified from Gall et al., (2003) composed of the following (in mM): 126 K-gluconate,

4 NaCl, 15 glucose, 5 HEPES, 1 MgSO₄, 0.15 BAPTA, and 0.05 CaCl₂, pH 7.3, via KOH, with 5 di-tris-creatine phosphate, 2 Tris-ATP, and 0.5 Na-GTP added from fresh frozen stock each day. The bath solution was carbogen-bubbled aCSF maintained at 32°C. A holding current of less than 10 pA was applied to maintain a holding potential of −70 mV. Input resistance was determined by hyperpolarizing cells with injections of 0 to −8 pA currents in five steps at an increment of −2 pA. Cerebellar granule cell excitability was measured by depolarizing cells from −70 mV with 1 s steps of currents of 0–16 pA in 2 pA increments. Spike events were detected and analyzed with pClamp 10.5 software (Axon, Molecular Devices).

Chemicals and proteins

Chemical compounds were obtained from Sigma-Aldrich unless otherwise indicated. Drugs were either bath-applied or infused directly through the electrode with the 2PK + Perfusion System (ALA Scientific; Zhan et al., 2020). Drugs were applied at the following concentrations: 30 μM (E)-2-benzylidene-3-(cyclohexylamino)-2,3-dihydro-1H-inden-1-one (BCI), 0.1 μg/ml MEK1-activated extracellular signal-regulated kinase 1 and 2 (pERK1/2; SignalChem Biotech), 1 μM TTA-P2 (Alomone Labs), 1 μM mibefradil (Sigma-Aldrich), and 3 mM okadaic acid (Sigma-Aldrich). FMRP(1–297)-tat was prepared as previously described (Zhan et al., 2020) and was added to the external medium of KO cells for 7–8 h, or delivered in vivo by tail vein injection 24 h before tests (Zhan et al., 2020).

Immunoprecipitation (IP) and coimmunoprecipitation (co-IP)

Protein–protein associations and phosphorylation of the Cav3-Kv4 complex were tested at different levels of [K]_o with co-IP and IP as described previously (Zhan et al., 2020). Transfected tsA-201 cells were washed with a low [K]_o (LK) solution composed of the following (in mM), 148 NaCl, 1 KCl, 10 HEPES, 3 CaCl₂, 1 MgCl₂, and 10 glucose, and equilibrated in LK solution for 10 min. Cells were then exposed to a high [K]_o (HK) solution composed of the following (mM), 148 NaCl, 50 KCl, 10 HEPES, 3 CaCl₂, 1 MgCl₂, and 10 glucose, for 5 min before being lysed in lysis buffer containing the following (in mM), 150 NaCl, 50 Tris, and 2.5 EGTA, 1% NP-40, pH 7.5, phosphatase inhibitor (Sigma-Aldrich, catalog #P5726) and proteinase inhibitor (Roche, catalog #04693124001). Lysates containing 500 μg total protein were incubated at 4°C for 2–3 h with one of the following antibodies: rabbit anti-Cav3.1 [1:50, custom made and lab verified (Molineux et al., 2006)], rabbit anti-Kv4.3 (1:50, Abcam, catalog #ab65794, RRID:AB_1140929), mouse anti-KChIP3 (1:50, NeuroMab, catalog #K66/38, RRID:AB_2877337), rabbit normal IgG (as a control, Abcam, Cat. ab172730, RRID:AB_2687931), mouse normal IgG (as a control, Abcam, catalog #ab37355, RRID:AB_2665484), rabbit anti-P-MAPK substrate (1:50, Cell Signaling Technology, catalog #14,378 s, RRID:AB_2798468), and rabbit anti-P-MAPK/CDK substrate (1:40, Cell Signaling Technology, catalog #2,325 s, RRID:AB_331820). The background control was used as a negative control by incubating lysate with normal IgG from the same species as the IP antibody. The immunocomplexes were then incubated with 30 μl protein G sepharose beads (GE healthCare Technologies, 17-0618-01), which were pre-equilibrated with lysis buffer at 4°C overnight. After four washes with lysis buffer, proteins were eluted from sepharose beads by boiling at 95–100°C for 5 min with 40 μl sample buffer diluted from 4× sample buffer (Bio-Rad, 1610747) with lysis buffer. IP samples were then resolved and analyzed with a Western blot. All commercially obtained antibodies were verified by suppliers. Full Western blot datasets are available for viewing on the repository Figshare: <https://figshare.com/s/402f8335aa1816cc35c4>.

Western blot

Cell lysates and IP samples were loaded to 6–12% SDS-polyacrylamide gel and resolved with SDS-PAGE. Proteins were transferred to a 0.2 μm PVDF membrane (Millipore) and probed with primary antibodies overnight at 4°C, followed by a goat anti-mouse (1:3,000, Invitrogen, catalog #62-6520, RRID:AB_2533947) or donkey anti-rabbit IgG (1:5,000, Cytiva, catalog #NA934-1 ml, RRID:RRID:AB_772206) HRP-conjugated secondary antibodies. Blot images were taken with a ChemiDoc Imager, and band densities were analyzed with Image Lab (Bio-Rad). Primary antibodies used in this study include rabbit anti-FMRP (1:1,000, Cell

Signaling Technology, catalog #7104 s, RRID:AB_10950502), mouse anti-FMRP (1:1000, Abcam, catalog #ab230915, RRID:AB_10950502), rabbit anti-pERK1/2 (1:1000, Cell Signaling Technology, catalog #4370 s, RRID:AB_2315112), rabbit anti-tERK1/2 (1:2000, Cell Signaling Technology, catalog #9102 s, RRID:AB_330744), mouse anti-GAPDH (1:2000, Invitrogen, catalog #39-8600, RRID:AB_2533438), rabbit anti-DUSP6 (1:1000, Abcam, catalog #ab76310, RRID:AB_1523517), and rabbit anti-αTubulin (1:2000, Abcam, catalog #ab176560, RRID:AB_2860019).

Experimental design and statistical analysis

When there were multiple samples in one experiment, samples were randomly chosen to receive different treatments. Experiments were performed with mouse genotypes and experimental groups known to the persons who conducted them. No experimental data without technical issues were excluded. The quantification of Western blot bands was conducted with the Image Lab software (Bio-Rad) by normalizing a target protein's intensity to housekeeping proteins. Patch-clamp recordings were analyzed with pClamp 10.5 software. All figures were prepared, and statistical analyses were performed with the OriginPro 8 or GraphPad Prism 6 and Adobe Illustrator CC 2021 software. Data normality was tested with the Shapiro–Wilk test. When normally distributed, statistical significance was determined using two-sample Student's *t* test for unpaired samples or Welch's test (*t* test with Welch correction) and a paired-sample Student's *t* test for the same samples under different conditions. When normality was rejected, the Mann–Whitney test was used for two-sample comparisons.

Results

Previous work established that the A-type current is subject to modulation by Cav3 T-type calcium current, with a primary effect of modulating the voltage for half inactivation (*V*_h) of Kv4 channels and thus the availability of *I*_A (Anderson et al., 2010a; Heath et al., 2014). The calcium dependence imparted on Kv4 channels is readily apparent when a reduction of Cav3 channel conductance produces a negative shift in Kv4 *V*_h, a process that reduces the amplitude of *I*_A (Anderson et al., 2010a,b, 2013; Heath et al., 2014). In the case of cerebellar granule cells, the Cav3-Kv4-KChIP3 complex has been shown to increase the spike output in relation to LTP of mossy fiber inputs (Heath et al., 2014; Rizwan et al., 2016; Zhan et al., 2020).

FMRP was recently found to exhibit co-IP and FRET with both Cav3.1 and Kv4.3 (Zhan et al., 2020), suggesting a direct association between FMRP and at least these two members of the Cav3-Kv4-KChIP3 complex. Importantly, these protein–protein interactions can be reproduced in tsA-201 cells by coexpressing cDNA for the principal subunits of Cav3.1-Kv4.3-KChIP3 (Anderson et al., 2010a,b, 2013). To further test the molecular interactions between FMRP and subunits of the complex, we first transiently transfected cDNA for human Cav3.1, Kv4.3, and KChIP3 in native tsA-201 cells that express FMRP (WT) or cells in which FMRP was knocked out by CRISPR–Cas9 technology (KO; Extended Data Figs. 1–2, 1–3). Kv4.3 *V*_h was measured using a series of step commands (1 s) from a holding potential of −90 mV to +60 mV in 10 mV increments followed by a step back to −30 mV (500 msec).

Cav3.1 and FMRP regulate Kv4.3 availability

We verified the ability for calcium to modulate Kv4.3 *V*_h by first constructing voltage-inactivation plots for Kv4.3 current in a medium containing 0 calcium (Fig. 1A). The addition of 1.5 mM calcium to the bathing medium resulted in a positive shift in Kv4.3 *V*_h (0 Ca²⁺, −55.5 ± 1.9 mV; 1.5 Ca²⁺, −49.9 ± 1.8 mV; *n* = 6; *p* = 0.001; paired *t* test) and an average 142 ± 33.3% (*n* = 5; *p* = 0.013; paired *t* test) increase in current

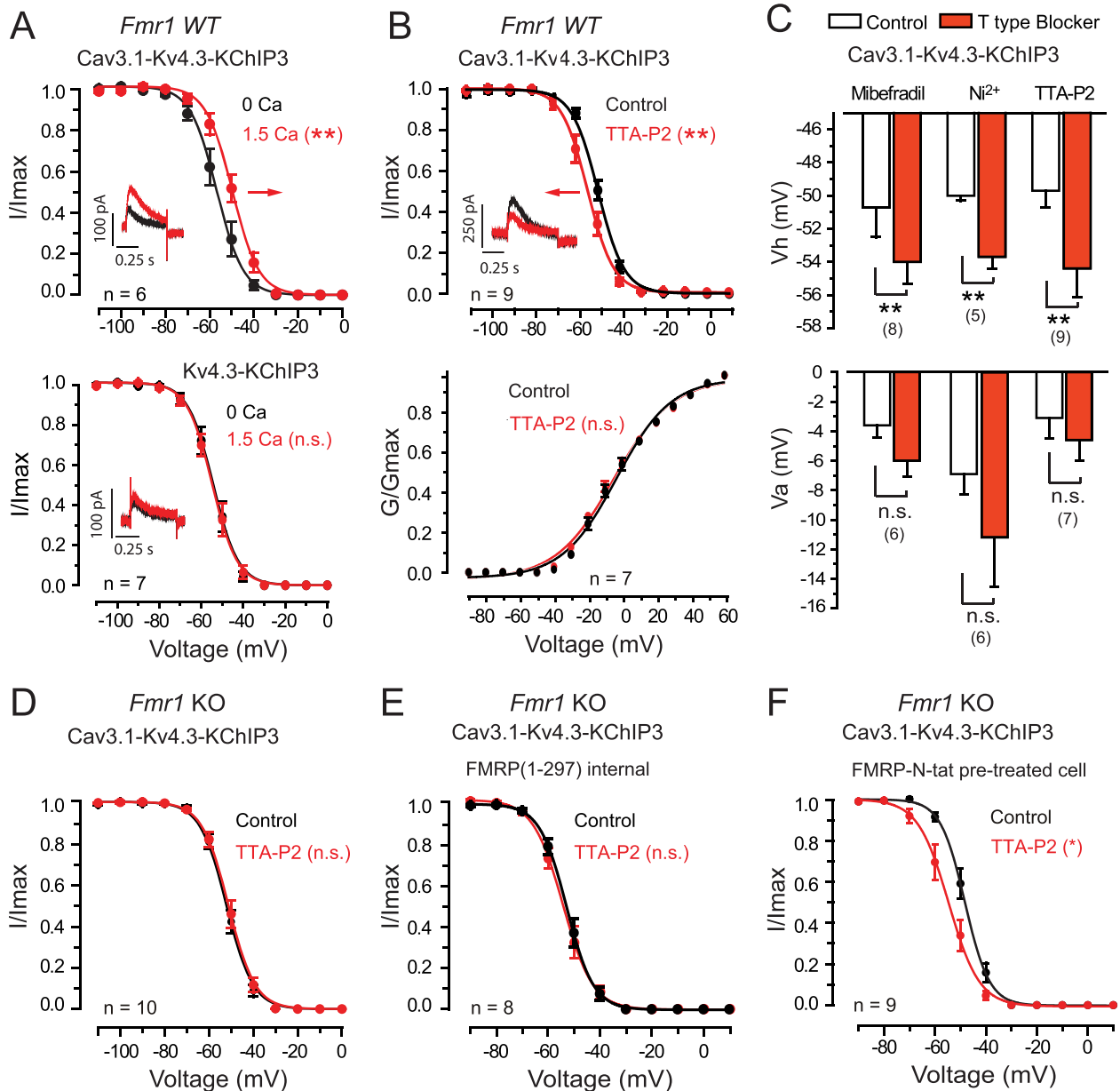


Figure 1. Cav3.1-induced shifts in Kv4.3 V_h are bidirectional and depend on the expression of FMRP. Shown in this and subsequent figures are mean voltage-inactivation or voltage-activation plots for Kv4.3 in *Fmr1* WT cells that express FMRP or in *Fmr1* KO cells in which FMRP was knocked out by CRISPR-Cas9. The proteins coexpressed in each test are indicated above the plots. Insets in **A** and **B** show superimposed records of Kv4.3 current evoked by a step from -40 mV to -30 mV before and after the indicated tests. **A**, Raising external calcium from 0 to 1.5 mM induces a positive shift of Kv4.3 V_h (arrow) and an increase in Kv4.3 current amplitude that does not occur in the absence of Cav3.1 expression. **B**, Blocking Cav3.1 conductance with 1 μ M TTA-P2 induces a negative shift of Kv4.3 V_h (arrow), but does not affect the steady-state activation of Kv4.3. **C**, Mean bar plots comparing the effects of three Cav3 channel blockers (1 μ M mibefradil, 300 μ M Ni²⁺, 1 μ M TTA-P2) establish the ability to selectively induce a negative shift of Kv4.3 V_h but not V_a when applied in a bathing medium containing 1.5 mM calcium. **D**, In *Fmr1* KO cells, TTA-P2 (1 μ M) fails to shift Kv4.3 V_h. **E**, **F**, A TTA-P2-induced negative shift in Kv4.3 V_h is not enabled in *Fmr1* KO cells by including 3 nM FMRP(1-297) in the pipette (**E**) but is produced by long-term preincubation (4–8 h) with 70 nM FMRP-N-tat (**F**). Average values are mean \pm SEM with sample values (*n*) indicated on plots. n.s., not significant, ***p* < 0.01, paired-sample *t* test. See also Extended Data Figures 1-1-1-3.

amplitude for a step of -40 to -30 mV (Fig. 1A). Both the calcium-induced shift in Kv4.3 V_h and increase in *I*_A amplitude were blocked by omitting Cav3.1 cDNA from the transfection (Fig. 1A). Conversely, applying 1 μ M TTA-P2 as a selective Cav3 channel blocker in a normal bathing medium containing 1.5 mM calcium negatively shifted Kv4.3 V_h (control, -49.7 ± 1.0 mV; TTA-P2, -54.4 ± 1.7 mV; *n* = 9; *p* = 0.003; paired *t* test) without affecting Kv4.3 voltage for activation (V_a; *n* = 7; *p* = 0.124; paired *t* test; Fig. 1B). The effects of TTA-P2 on Kv4.3 V_h were further reflected in a $42 \pm 7.4\%$ (*n* = 9; *p* = 4.5×10^{-4} ; paired *t* test) decrease

in *I*_A amplitude for a step from -40 to -30 mV (Fig. 1B). The negative shift in Kv4.3 V_h induced by TTA-P2 was comparable to that obtained in 1.5 mM calcium medium for the application of either 1 μ M mibefradil or 300 μ M Ni²⁺, with no significant effects on Kv4.3 V_a (Fig. 1C; Anderson et al., 2010a).

We note that much of the work to date on the Cav3-Kv4-KChIP3 complex was conducted in cerebellar granule cells or WT tsA-201 cells that express FMRP. To test the role of FMRP, we used the *Fmr1* KO cell line. Using KO cells, we found that in the absence of FMRP, the ability of TTA-P2 application to

induce a negative shift in Kv4.3 Vh in cells was lost (Fig. 1D). To further test the effects of a loss of FMRP, we recorded the Kv4.3 current in KO cells coexpressing the Cav3.1-Kv4.3-KChIP3 complex in the standard internal electrode solution or in the presence of 3 nM FMRP(1–297) in the recording electrode. In the presence of internal 3 nM FMRP(1–297), we found no effect of applying 1 μ M TTA-P2 on Kv4.3 Vh (Fig. 1E). We considered the possibility that reinstating FMRP functions in KO cells might require more time than the typical 10–15 min whole-cell recordings. It was previously shown that attaching the cell-permeating *tat*-peptide moiety to FMRP(1–297; FMRP-N-*tat*) facilitates its passage across cell membranes (Zhan et al., 2020). We thus pretreated KO cells coexpressing Cav3.1-Kv4.3-KChIP3 with 70 nM FMRP-N-*tat* in the cell medium and found variable levels of recovery at 4 h but full recovery at 7 h. When recordings were subsequently conducted in these cells, the Kv4.3 Vh was not changed between FMRP-N-*tat* pretreated cells to those without this treatment ($p = 0.07$; Fig. 1D,F). However, in cells pretreated for the longer time frame with FMRP-N-*tat*, applying 1 μ M TTA-P2 now induced a significant negative shift in Kv4.3 Vh (KO, -48.1 ± 1.4 mV; KO post-TTA-P2, -54.8 ± 2.1 mV; $n = 9$; $p = 0.012$; paired *t* test; Fig. 1F).

Together these tests are important in providing the first evidence that Cav3 calcium conductance can induce a bidirectional shift in Kv4.3 Vh and I_A amplitude in cells expressing the Cav3-Kv4-KChIP3 complex. Moreover, the Cav3.1 calcium-dependent modulation of Kv4.3 Vh unexpectedly depends on the expression of FMRP, identifying a key role for this molecule in the complex. The ability for FMRP-N-*tat* to rescue the calcium-dependent modulation of Kv4.3 in KO cells further indicates that the N-terminal portion of FMRP is sufficient to reinstate the normal functions of the Cav3-Kv4 complex.

Cav3.1 and KChIP3 are necessary to induce a calcium-dependent modulation of Kv4 Vh

It is known that KChIP molecules can act as the calcium sensor for Kv4 channels with four KChIP subunits present in an assembled channel (An et al., 2000; Vierra and Trimmer, 2022) and EF hands 3 and 4 available to bind calcium. Yet the exact role for KChIP3 in Cav3-dependent modulation of Kv4 channels has not been determined.

To test the role of KChIP3, we first coexpressed Cav3.1 and Kv4.3 without KChIP3. In this case applying TTA-P2 (1 μ M) produced a very slight shift in Kv4.3 Vh (control, -48.6 ± 1.2 mV; TTA-P2, -49.7 ± 1.1 mV; $n = 10$; $p = 0.003$; paired *t* test; Fig. 2A, B). However, coexpressing KChIP3 with Cav3.1-Kv4.3 restored the ability of TTA-P2 application to induce a much larger negative shift in Kv4.3 Vh (-4.8 ± 3.4 mV; $n = 9$; $p = 0.005$; two-sample *t* test; Fig. 2B). The effect of TTA-P2 was lost if an interfering peptide *tat*-pp1 (10 μ g/ml) that impedes the Kv4.3-KChIP3 interaction (Scannevin et al., 2004; Callsen et al., 2005) was preapplied in the bath solution (Fig. 2B). We further tested the role of specific EF hands by coexpressing KChIP3 constructs that were mutated to block the function in EF hand 3 (KChIP3_(E186Q)), EF hand 4 (KChIP3_(E234Q)), or both. Neither the two single KChIP3 mutants expressed alone with Cav3.1-Kv4.3 fully prevented a TTA-P2-induced negative shift in Kv4.3 Vh (Fig. 2C). Coexpressing Cav3.1-Kv4.3 and the double mutant KChIP3_(E186Q, E234Q) had no effect on the resting value of Kv4.3 Vh (WT Cav3.1-Kv4.3-KChIP3 Vh, -49.7 ± 1.0 mV; $n = 9$; WT Cav3.1-Kv4.3-KChIP3_(E186Q, E234Q) Vh, -48.5 ± 0.6 mV; $n = 8$; $p = 0.334$; Welch's test) but proved to fully block any effects of applying TTA-P2 on Kv4.3 Vh (Fig. 2C). These data confirm

that calcium sensitivity of the Cav3-Kv4 complex also requires the actions of EF hands 3 and 4 of KChIP3.

Previous work established that FMRP forms a link to both Cav3.1 and Kv4.3 (Zhan et al., 2020). To determine if FMRP forms a similar close relationship to KChIP3 as the calcium-sensing component of the complex, we conducted co-IP tests in WT cells. These experiments established that FMRP also co-IPs with KChIP3 (Fig. 2E; Extended Data Fig. 2-1). To determine if membrane depolarization and Cav3.1 calcium influx induced any calcium-dependent change in the relationship between KChIP3 and other members of the complex, we compared co-IPs obtained in the presence of 1 mM [K]_o (LK) or 50 mM [K]_o (HK) solution to promote Cav3.1 calcium influx. HK solution promoted a selective and striking loss of the co-IP between KChIP3 and FMRP (Fig. 2E) but not between KChIP3 and either Kv4.3 or Cav3.1 (Extended Data Fig. 2-1).

To explore the functional outcome of KChIP3 and FMRP on Kv4 Vh, we tested the effects of different levels of internal calcium concentration and with or without FMRP. By coexpressing Kv4.3-KChIP3 in the absence of Cav3.1 and buffering internal calcium concentration to 0 μ M (MaxChelator), we determined that adding KChIP3 had no effect on the baseline value of Kv4 Vh in either WT or KO cells (Fig. 2F). We then repeated these tests by coexpressing Kv4.3-KChIP3 and recorded with internal solutions that had calcium concentrations buffered to either 0 or 13 μ M to compare Kv4 Vh. In WT cells, a higher internal calcium concentration induced a significant positive shift in Kv4 Vh (WT 0 calcium, -40.4 ± 1.5 mV; $n = 10$; 13 μ M calcium, -16.9 ± 1.0 mV; $n = 7$; $p = 5.3 \times 10^{-9}$; two-sample *t* test; Fig. 2G). However, repeating these tests in *Fmr1* KO cells revealed no calcium-dependent shift in Kv4 Vh in the presence of elevated internal calcium (KO 0 calcium, -39.2 ± 2.0 mV; $n = 8$; 13 μ M calcium, -41.2 ± 2.3 mV; $n = 9$; $p = 0.64$; two-sample *t* test; Fig. 2G), indicating that FMRP is required to invoke a calcium-dependent positive shift in Kv4 Vh.

Together, these tests are important in indicating that Cav3 calcium-induced shifts in Kv4.3 Vh and the modulation of I_A amplitude depend on all of Cav3.1, KChIP3, and FMRP, with a selective and dynamic change in the FMRP-KChIP3 association with an elevation of internal [Ca].

Cav3.1 and FMRP regulate ERK phosphorylation

We previously found that a negative shift in Kv4 channel Vh in cerebellar granule cells invoked by mossy fiber stimulation could be prevented by PD-98059, an inhibitor of mitogen-activated protein kinase kinase that phosphorylates and activates ERK (Rizwan et al., 2016). Yet the factors that control ERK activation and the potential target(s) for ERK phosphorylation of subunits in the Cav3-Kv4-KChIP3 complex are unknown. ERK has been shown to phosphorylate three different sites on Kv4.2 that can cause shifts in Vh or Va to regulate I_A availability (Adams et al., 2000; Schrader et al., 2002, 2006), but the potential actions of ERK on Kv4.3 have not been reported. Interestingly, Cav3.1-mediated calcium influx has been reported to decrease ERK activation in HEK293 cells (Choi et al., 2005).

To define any Cav3-mediated regulation of the complex by ERK, we coexpressed Cav3.1-Kv4.3-KChIP3 in WT cells and used Western blots to detect the effects of membrane depolarization and calcium conductance on ERK1/2 (ERK) activation. For this, we used an antibody that targets phosphorylated ERK (pERK) to identify the level of pERK in relation to total ERK (tERK; Fig. 3A). These tests established a baseline ratio of pERK/tERK in LK (1.5 mM) and that application of HK

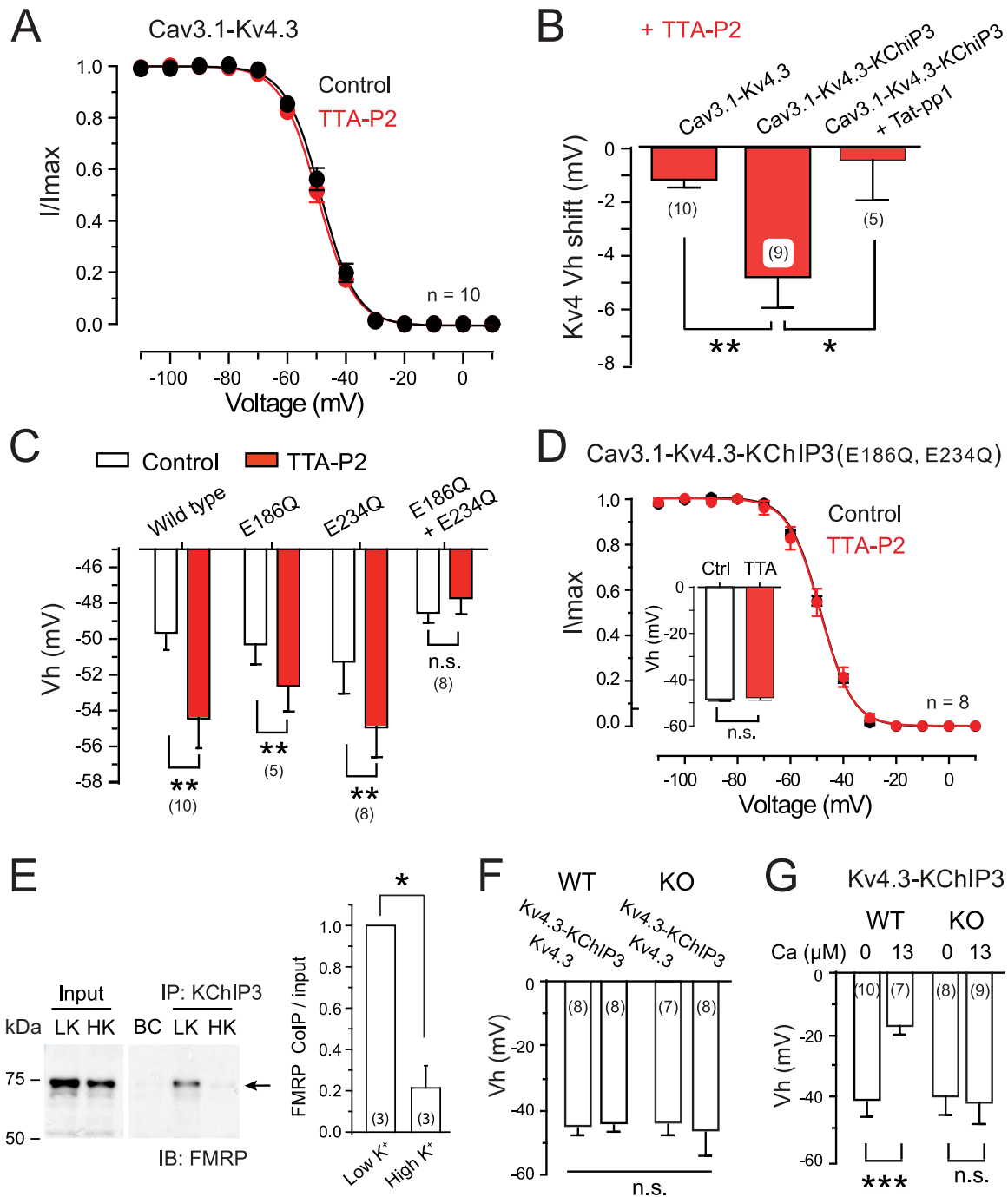


Figure 2. KChIP3 and FMRP are required to enable a calcium-dependent shift in Kv4 Vh. Shown are the effects of TTA-P2 application (A–D) on *Fmr1* WT cells coexpressing the indicated subunits. **A, B**, In the absence of KChIP3 coexpression, TTA-P2 has only a small effect on Kv4.3 Vh (A, B). Coexpressing KChIP3 restores a larger TTA-P2-induced negative shift in Kv4.3 Vh that is lost if preincubated cells with a *tat-pp1* peptide that interferes with the KChIP3–Kv4.3 binding site (B). **C, D**, Mean bar plots showing a TTA-P2–induced shift in Kv4.3 Vh are partially blocked in cells expressing either EF hand mutant and fully blocked upon expression of a dual KChIP3 EF hand mutant. **E**, Western blot and mean bar plots showing co-IP between KChIP3 and FMRP in *Fmr1* WT cells expressing all subunits of the Cav3–Kv4 complex. The KChIP3–FMRP co-IP detected in the presence of 1.5 mM [K]o (LK) is lost in the presence of 50 mM [K]o (HK) medium to promote Cav3.1 calcium influx. **F**, Coexpressing Kv4.3–KChIP3 in the absence of Cav3.1 has no effect on Kv4.3 Vh in *Fmr1* WT or *Fmr1* KO cells (0 μM internal free calcium, MaxChelator). **G**, Coexpressing Kv4.3–KChIP3 in the absence of Cav3.1 reveals that recording in the presence of 13 μM calcium in the electrode induces a positive shift in Kv4 Vh in *Fmr1* WT cells but not in *Fmr1* KO cells (G). **B, C**, Background control. Average values are mean \pm SEM with sample sizes (n) indicated in brackets. n.s., not significant; * $p < 0.05$; ** $p < 0.01$; *** $p < 0.001$; paired-sample t test (C, D) and two-sample t test (B, F, G). See also Extended Data Figure 2-1.

decreased the pERK/terk ratio by 53.7% within 10 min (HK, 0.46 ± 0.08 ; $n = 7$; $p = 4.75 \times 10^{-4}$; paired t test; Fig. 3A). Moreover, this HK-induced reduction in pERK was blocked by preincubation in 1 μM TTA-P2 (HK, 0.97 ± 0.28 ; $n = 4$; $p = 0.927$; paired t test; Fig. 3B), indicating that a depolarization-induced reduction of

pERK depends on Cav3.1 calcium conductance. Repeating these tests in KO cells expressing Cav3.1–Kv4.3–KChIP3 further revealed that the HK-induced reduction in pERK levels was lost in the absence of FMRP (KO HK, 0.91 ± 0.10 ; $n = 4$; $p = 0.422$; paired t test; Fig. 3C).

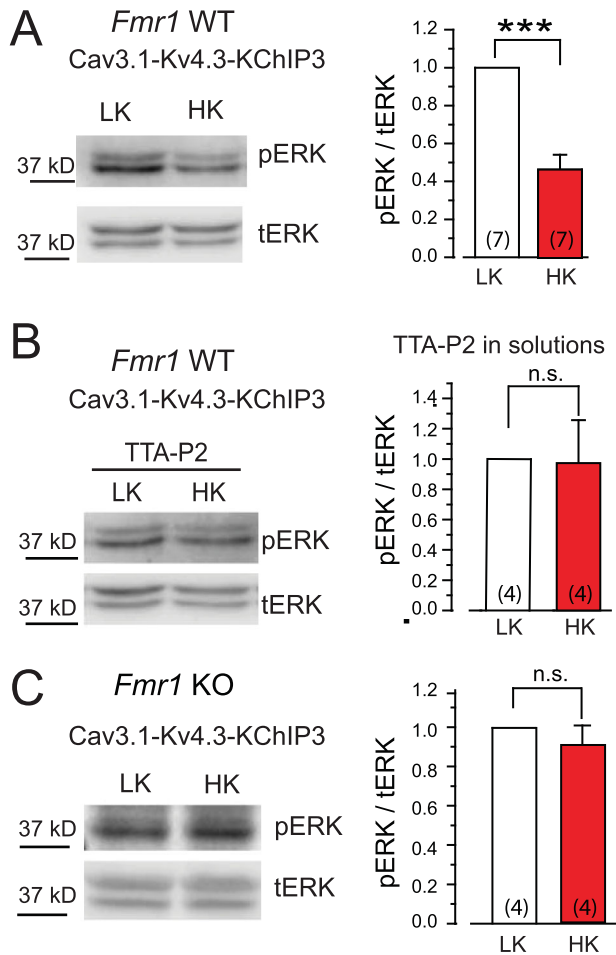


Figure 3. A Cav3.1-dependent reduction in pERK is impaired in *Fmr1* KO cells. Shown are the levels of pERK in relation to tERK at rest and upon depolarization in tsA-201 cells expressing Cav3.1-Kv4.3-KChIP3. pERK levels are quantified by the Western blot and mean bar plots in the presence of 1.5 mM [K]_o (LK) or 50 mM [K]_o (HK) medium. **A**, In WT cells a resting level of pERK is detected in LK medium. The pERK/tERK ratio is reduced over 10 min upon depolarization in an HK medium. **B**, The decrease in pERK/tERK with HK-induced depolarization is prevented if Cav3.1 conductance is blocked by preincubation in 1 μ M TTA-P2. **C**, The HK-induced reduction of pERK levels is absent in *Fmr1* KO cells. All cells in **A–C** were also transfected with 0.7 μ g Kir2.1 to maintain a negative resting potential. Average values are mean \pm SEM with sample sizes (*n*) indicated in bar plots. n.s., not significant; ****p* < 0.001; Student's paired-sample *t* test.

These data establish that Cav3.1 calcium conductance lowers the level of activated ERK and that this process requires the expression of FMRP.

Cav3.1 activates DUSP to regulate ERK and set Kv4.3 availability

A Cav3.1-mediated reduction in pERK levels could contribute to a shift in Kv4.3 Vh and I_A availability. To test this, we recorded from WT cells expressing Cav3.1-Kv4.3-KChIP3 with or without 1 μ M TTA-P2 in the bath and measured Kv4.3 Vh. For this Kv4.3 current was first measured using a control internal electrolyte that was subsequently replaced by direct electrode infusion with an electrolyte containing 0.2 μ g/ml pERK (Fig. 4A). When Cav3.1 conductance was blocked in the presence of 1 μ M TTA-P2 in the bath, the infusion of pERK induced a significant negative shift in Kv4.3 Vh ($n = 6$; $p = 0.011$; paired *t* test; Fig. 4A). However, when Cav3.1 conductance was intact (no TTA-P2 in medium), internal infusion of pERK had no significant effect

on Kv4.3 Vh ($n = 3$; $p = 0.311$; paired *t* test; Fig. 4A). These results are important in suggesting that Cav3.1 calcium conductance can occlude the actions of pERK even when added directly to the electrolyte. To assess the requirement for FMRP in these results, we coexpressed the complex in KO cells in the presence of 1 μ M TTA-P2 in the bath to prevent calcium conductance and found that recording with 0.2 μ g/ml pERK in the electrode again significantly negatively shifted the Kv4.3 Vh (control, -45.7 ± 1.8 mV; $n = 6$; pERK1/2, -53.6 ± 1.5 mV; $n = 8$; $p = 0.0069$; two-sample *t* test; Fig. 4B). Together, these results indicate the ability for pERK to induce a negative shift in Kv4.3 Vh through a process that is actively prevented or reduced by Cav3.1 calcium conductance.

Cav3.1 calcium influx might reduce pERK levels by activating a phosphatase to dephosphorylate ERK to reduce its actions on downstream targets at serine/threonine (Ser/Thr) sites. The process of dephosphorylation is most often achieved by Ser/Thr phosphatases that include PP1/PP2A (Narayanan et al., 2007). Indeed, Cav3 calcium conductance has been associated with the activation of PP2A (Ferron et al., 2011), and PP2A has been shown to dephosphorylate all of FMRP (Narayanan et al., 2007), ERK (Kim et al., 2008), or S6K1 (Hahn et al., 2010). To test the role of PP2A, we coexpressed the Cav3.1-Kv4.3-KChIP3 complex in WT cells in the presence of 3 nM okadaic acid to block PP1 and PP2A. We then applied 1 μ M TTA-P2 to block Cav3.1 conductance and still found a negative shift in Kv4.3 Vh (control, -46.8 ± 1.4 mV; TTA-P2, -52.2 ± 1.2 mV; $n = 5$; $p = 4.98 \times 10^{-5}$; paired *t* test; Fig. 4C).

A key factor that specifically controls pERK levels is the family of DUSP that dephosphorylate phosphothreonine and phosphotyrosine residues on MAPK (Caunt et al., 2008). To test the potential role of DUSPs, we coexpressed the Cav3.1-Kv4.3-KChIP3 complex in WT cells and recorded it in the presence of 30 μ M BCI as an allosteric inhibitor of DUSP1/6 (Molina et al., 2009). Under these conditions, the perfusion of 1 μ M TTA-P2 had no effect on Kv4.3 Vh (control, -55.7 ± 1.7 mV; TTA-P2, -56.6 ± 1.6 mV; $n = 7$; $p = 0.12$; paired *t* test; Fig. 4D), revealing that BCI occluded the effects of Cav3.1 conductance on Kv4.3. In contrast, when Cav3.1-Kv4.3-KChIP3 was coexpressed in WT cells, 30 μ M BCI application by itself produced a significant negative shift in Kv4.3 Vh (control, -49.8 ± 0.7 mV; BCI, -54.6 ± 1.0 mV; $n = 9$; $p = 9.8 \times 10^{-6}$; paired *t* test; Fig. 4E). In fact, the BCI-induced negative shift in Kv4.3 Vh was not significantly different from that induced by TTA-P2 (BCI Vh shift, -4.8 ± 0.5 mV; $n = 9$; TTA-P2 Vh shift, -4.8 ± 1.1 mV; $n = 9$; $p = 0.99$). These results were important in revealing that a Cav3.1-mediated positive shift in Kv4.3 Vh (compare Fig. 1A) involves Cav3.1 activation of DUSP1/6 and its influence on pERK. This conclusion was further verified using Western blots to repeat the test of depolarizing WT cells using an HK medium (compare Fig. 3), which revealed that inhibiting DUSP1/6 with 30 μ M BCI prevented an HK-induced depolarization from reducing the pERK/tERK ratio (Fig. 4F).

We further explored the extent to which these results could be reproduced by an increase in [Ca]_i (Fig. 4G). Using whole-cell recordings in WT cells coexpressing only Kv4.3-KChIP3, we buffered [Ca] in the electrode (MaxChelator) to either 0 or 13 μ M. Cells recorded in the presence of 13 μ M internal calcium exhibited a positive shift in Kv4.3 Vh (Fig. 4G). However, no effect on Kv4.3 Vh was detected under these conditions in the presence of 30 μ M BCI to block DUSP1/6 (Fig. 4G).

These results reveal that a Cav3.1-mediated activation of DUSP1/6 that downregulates the level of pERK is accompanied by a positive shift in Kv4.3 Vh that will increase I_A .

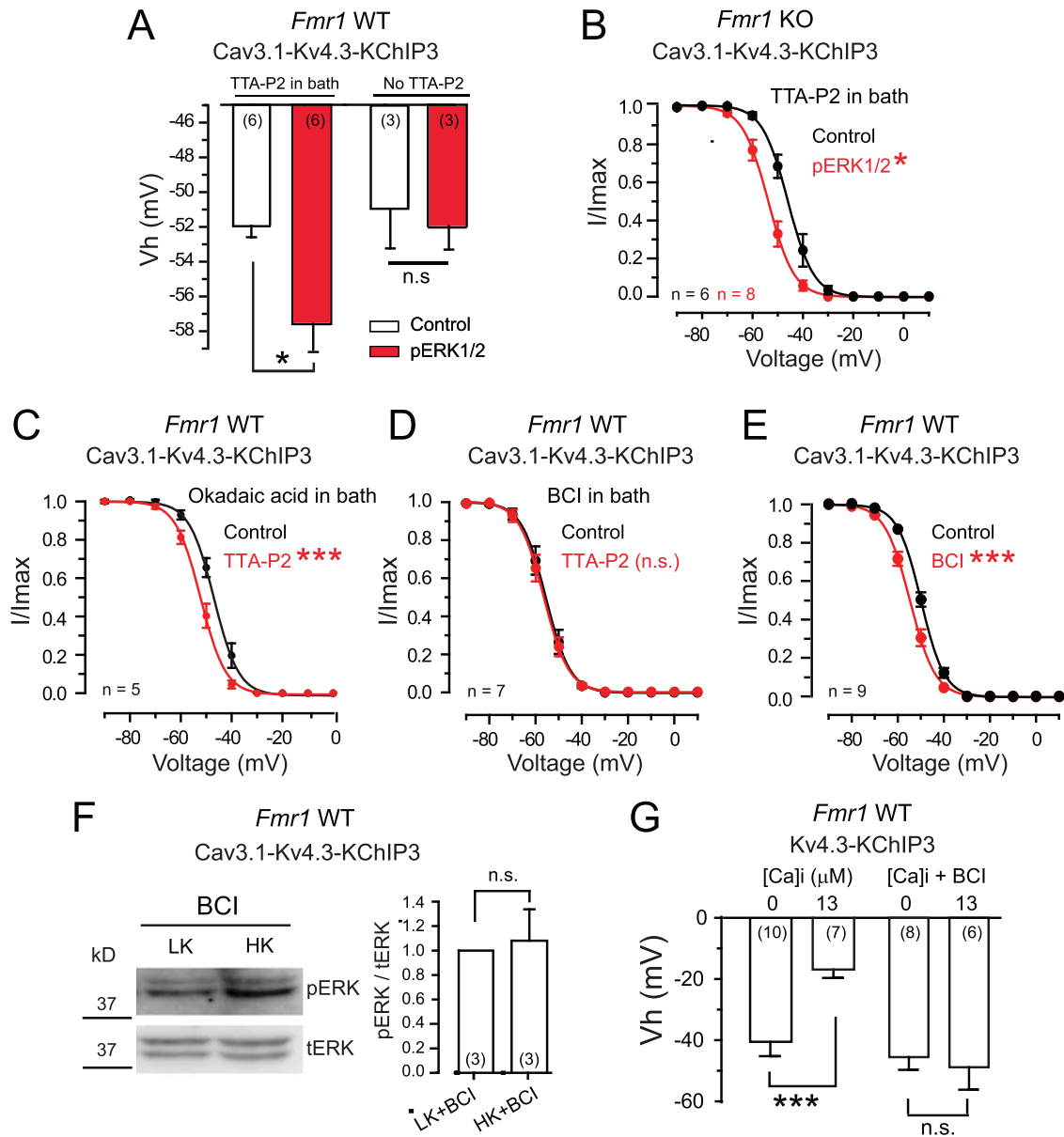


Figure 4. Cav3.1 calcium influx activates DUSP to regulate pERK actions on Kv4.3 Vh. Shown are results from whole-cell recordings and Western blots from *Fmr1* WT or KO cells expressing the indicated subunits. **A, B**, The effects of direct pERK infusion through the electrode in *Fmr1* WT (**A**) or *Fmr1* KO cells (**B**) with Cav3.1-Kv4.3-KChIP3 subunits coexpressed. With 1 μ M TTA-P2 in the bath to block T-type current, direct infusion of pERK results in a negative shift in Kv4.3 Vh in both *Fmr1* WT and KO cells. However, pERK has no effect in the absence of TTA-P2 to retain Cav3.1 conductance (**A**). **C–E**, The effects of phosphatase blockers on Kv4.3 Vh. Bath application of 1 μ M TTA-P2 induces a negative shift in Kv4.3 Vh in the presence of 3 nM okadaic acid to block PP1/PP2A phosphatases (**C**), but not in the presence of 30 μ M BCI to block DUSP1/6 (**D**). Recordings in the presence of 30 μ M BCI also exhibit a negative shift in Kv4.3 Vh (**E**). **F**, Western blots indicating that BCI (30 μ M) in the bath blocks a reduction of pERK normally stimulated by an HK-mediated depolarization (HK) in *Fmr1* WT cells expressing the complex (compare Fig. 3A). **G**, The effects of blocking DUSP1/6 on Kv4.3 Vh in the absence of Cav3.1 expression and direct manipulation of internal calcium concentration in the electrode. Recording with a high level of buffered internal calcium (13 μ M, MaxChelator) in the electrode produces a positive shift in Kv4.3 Vh that is blocked in the presence of 30 μ M BCI in the bath to block DUSP1/6. Average values are mean \pm SEM with sample sizes (*n*) indicated in bar plots. n.s., not significant; * p < 0.05; *** p < 0.001; Student's paired-sample *t* test (**A, C–F**) and Student's two-sample *t* test (**B, G**).

Depolarization induces differential effects of phosphorylation of Kv4.3 and FMRP

While the previous data revealed that a Cav3.1-DUSP-ERK signaling pathway regulates calcium dependence of the Cav3-Kv4 complex, the actual targets of ERK-mediated phosphorylation in this process are unknown. The tests already conducted enable predictions on what elements may be important. While the regulation of Cav3 channel isoforms by ERK has been reported in fibroblasts and cardiomyocytes (Sharma et al., 2023), we have not detected any change in Cav3.1 density or voltage dependence in relation to stimuli that modulate the Cav3-Kv4 complex

(Heath et al., 2014; Rizwan et al., 2016; Zhan et al., 2020). Several lines of evidence implicate Kv4.3 as one important target for phosphorylation. Specifically, shifts in Kv4.3 Vh could be induced in WT cells by direct infusion of pERK in the presence of TTA-P2 to block Cav3.1 conductance (Fig. 4A) or with a direct increase in [Ca]_i in the absence of Cav3.1 expression (Fig. 4G). A negative shift in Kv4.3 Vh could also be induced by internal pERK infusion in WT cells expressing only Cav3.1-Kv4.3 (Fig. 4A), suggesting that KChIP3 is not required as an ERK target to enable the calcium-dependent effects studied here. In KO cells coexpressing Cav3.1-Kv4.3-KChIP3 and that lack

FMRP, both the calcium-dependent negative shift in Kv4.3 Vh (Fig. 2G) and an HK-induced reduction in pERK levels (Fig. 3C) were lost, but the effects of pERK on Kv4.3 Vh remained (Fig. 4C). These results indicate that pERK actions on Kv4.3 can be sufficient to modulate Kv4.3 Vh but that FMRP is also required for regulating the actions of ERK that promote a calcium-dependent shift in Kv4.3 Vh.

ERK is a member of the MAPK family that can phosphorylate targets at either serine (PXS*P) or threonine (PXpTP) motifs (Rubinfeld and Seger, 2005). To identify targets for MAPK-mediated phosphorylation, we depolarized the WT cells

coexpressing Cav3.1-Kv4.3-KChIP3 using an HK medium. Cells were then processed for Western blot analysis for IP between proteins reactive for antibodies specific to MAPK phosphorylated serine (pSer) or threonine (pThr) motifs with each of Cav3.1, Kv4.3, KChIP3, and FMRP proteins (Fig. 5). These tests revealed pThr sites on FMRP in LK conditions but no detectable difference in phosphorylation levels between LK and HK conditions (Fig. 5A,B). No consistent pThr labeling was detected for any of Cav3.1, Kv4.3, or KChIP3 (Fig. 5A,B). Tests of IP for serine motifs revealed pSer labeling for both FMRP and Kv4.3 under resting conditions of an LK medium (Fig. 5C,D). The exposure

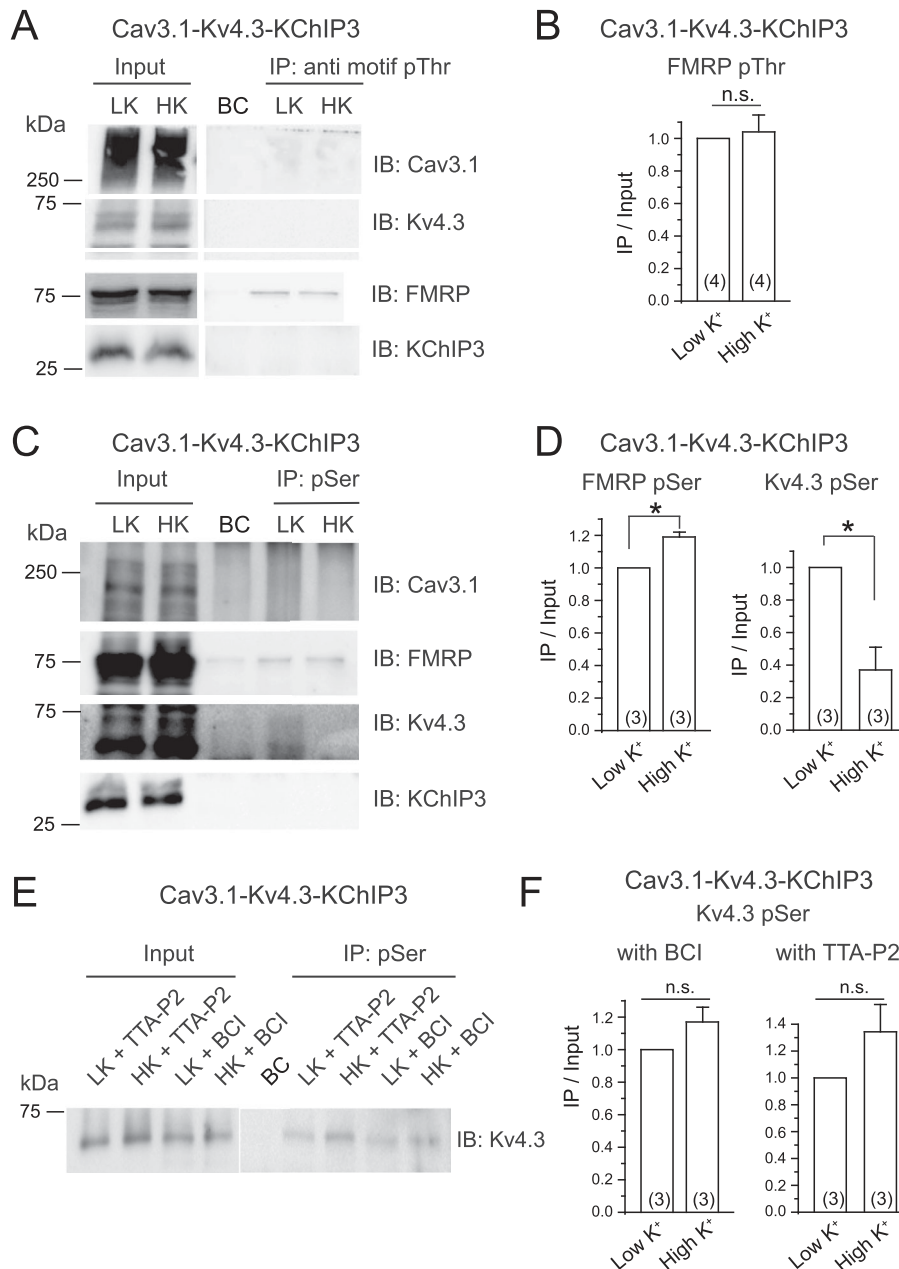


Figure 5. Cav3.1 calcium influx reduces Kv4.3 phosphorylation through a DUSP-ERK pathway. Shown are the effects of testing *Fmr1* WT cells coexpressing Cav3.1-Kv4.3-KChIP3 in either LK or HK on the phosphorylation of the indicated subunits. Results are shown in Western blots (**A**, **C**, **E**) and mean bar plots (**B**, **D**, **F**) of the indicated proteins after IP with different ERK substrate antibodies. **A**, **B**, An anti-PXpTP motif (pThr) antibody detects phosphorylation of FMRP (**A**), but the level of phosphorylated FMRP is not affected by HK treatment (**B**). **C**, **D**, An anti-PXS*P or S*PXK motif (pSer) antibody detects phosphorylation of both Kv4.3 and FMRP (**C**), with HK stimulation increasing the level of pSer on FMRP and decreasing the level on Kv4.3 (**D**). **E**, **F**, Representative Western blots (**E**) and mean bar plots of the extent of phosphorylation at pSer sites in LK versus HK conditions (**F**). Pretreating cells with 1 μ M TTA-P2 or 30 μ M BCI blocks the HK-induced reduction of Kv4.3 phosphorylation. Abbreviations: LK, low potassium; HK, high potassium; BC, background control; IP, immunoprecipitation; IB, immunoblotting. Average values are mean \pm SEM with sample sizes (*n*) indicated in bar plots. n.s., not significant; **p* < 0.05; Student's paired-sample *t* test.

of cells to an HK medium produced an increase in pSer labeling on FMRP and a marked decrease in phosphorylation of Kv4.3 (Fig. 5C,D). Repeating tests for the pSer motif of Kv4.3 further revealed that the reduction of Kv4.3 phosphorylation in an HK medium was prevented if cells were preincubated with either 1 μ M TTA-P2 (Fig. 5E) or 30 μ M BCI (Fig. 5F). The increase in FMRP phosphorylation was also correlated to Cav3.1 calcium influx although the exact mediator for phosphorylation is unknown since depolarization also lowers the levels of pERK (Fig. 3A).

These data reveal that FMRP is phosphorylated at both pSer and pThr sites and that depolarization increases the pSer labeling. pSer labeling on Kv4.3 is instead reduced upon depolarizing cells, a process that involves Cav3.1 activation of DUSP1/6 and its ability to dephosphorylate ERK. The data thus suggest that Cav3.1 activation of DUSP1/6 and modulation of FMRP and Kv4.3 phosphorylation enable KChIP3 to induce a depolarizing shift in Kv4.3 Vh that increases I_A in a calcium-dependent manner (compare Fig. 1A).

Hyperexcitability of cerebellar granule cells in *Fmr1* KO mice is rescued by FMRP-N-tat

Several aspects of excitability of cerebellar granule cells and their response to synaptic input have been shown to depend on the Cav3.1-Kv4-KChIP3 complex (Heath et al., 2014; Rizwan et al., 2016; Zhan et al., 2020). To further test the effects of FMRP-N-tat on excitability of neurons, we recorded from lobule 9 granule cells from P22–24 WT and *Fmr1* KO mice in cerebellar slices prepared 1 d following tail vein injection of either vehicle or 1 mg/kg FMRP-N-tat. Whole-cell recordings were used to deliver 1 s current pulses to map the current–frequency relationship of sodium spike discharge. In WT mice injected with vehicle alone, granule cells fired with an initial frequency of 0.5 ± 0.54 Hz, showing a linear increase in firing with increments of current injection up to 42.2 ± 8.7 Hz ($n = 9$; Fig. 6A,B). The maximum firing frequency reached during 16 pA current injection increased by 86% in *Fmr1* KO granule cells compared with WT cells, further indicating a state of hyperexcitability (Fig. 6C). An increased sensitivity to depolarizations was also apparent in a decrease in the rheobase to evoke spike firing in vehicle-injected *Fmr1* KO mice compared with in WT mice (Fig. 6D). Finally, the increased spike frequency was associated with a significant decrease in the decay tau (rate of repolarization) of evoked spikes (Fig. 6E). By comparison there was no significant difference in the input resistance of granule cells between WT and *Fmr1* KO mice (WT, 1.05 ± 0.10 G Ω ; $n = 9$; *Fmr1* KO, 1.30 ± 0.17 G Ω ; $n = 7$; $p = 0.24$; two-sample *t* test). We then injected *Fmr1* KO mice with 1 mg/kg FMRP-N-tat and prepared tissue slices 24 h later, a time previously shown to be sufficient for this compound to distribute throughout the cerebellum for uptake by granule and Purkinje cells (Zhan et al., 2020). Here we found complete rescue of the elevated firing rate of *Fmr1* KO compared with WT granule cells over the full range of a current–frequency plot, with similar effects on rheobase and rate of spike repolarization (Fig. 6A–E). These effects by FMRP-N-tat are important in that IA has previously been shown in granule cells to shape each of the parameters tested here (Heath et al., 2014; Zhan et al., 2020).

An imbalance in expression levels of DUSP in *Fmr1* KO cells is rescued by FMRP-N-tat

The function of the Cav3.1-DUSP-ERK signaling pathway here was defined primarily using WT or KO tsA-201 cells. To explore

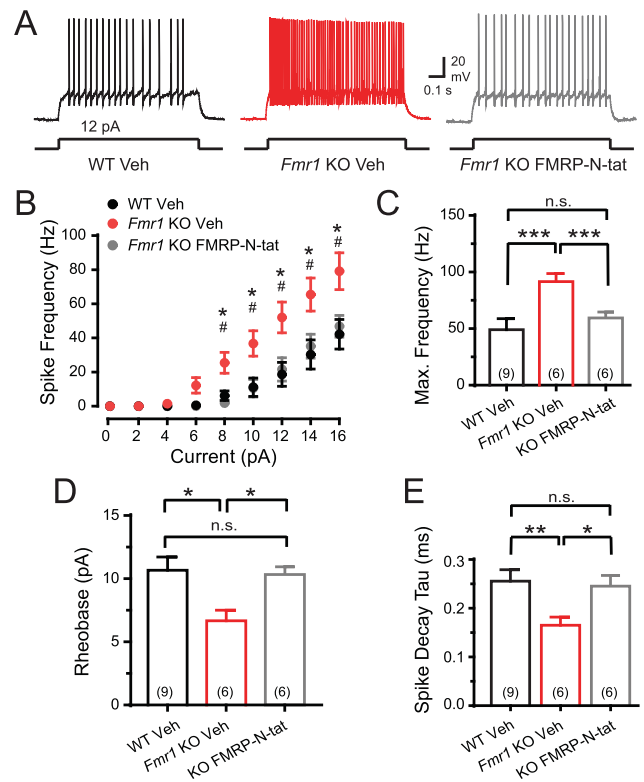


Figure 6. FMRP regulates excitability in cerebellar granule cells. The effects on spike output of cerebellar granule cells in tissue slices of P22–24 male WT and *Fmr1* KO mice 24 h following tail vein injection of vehicle or 1.0 mg/kg FMRP-N-tat. **A**, Representative whole-cell recordings indicate that tonic firing frequency in response to current injection is markedly elevated in vehicle-injected *Fmr1* KO mice compared with WT mice. Firing frequency is rescued in granule cells of *Fmr1* KO mice 24 h after FMRP-N-tat injection. **B**, Mean frequency–current (F/I) plots of spike output for 1-s-long current injections. **C**, Bar plots of mean maximal firing frequency measured from the first four spike outputs with 16 pA current injection. **D**, Bar plots of rheobase current required to reach spike firing threshold. **E**, Bar plots of mean decay tau of spike output as a measure of the rate of repolarization with the rheobase current injection required to trigger spike firing. Average values are mean \pm SEM with sample sizes (n) indicated in brackets. n.s., not significant; * $p < 0.05$, ** $p < 0.01$, and *** $p < 0.001$ (C–E); * $p < 0.05$ for *Fmr1* KO vehicle versus FMRP-N-tat injected firing rate (B); Student's two-sample *t* test.

the prevalence of DUSP6 expression in situ, we conducted immunocytochemical labeling for DUSP6 in the cerebellum of P60 male mice. These tests confirmed a widespread expression of this phosphatase in granule cells (Fig. 7A). The DUSP family is interesting in establishing a reciprocal inhibitory system with pERK that will activate nuclear transcription factors that modify DUSP levels (Rubinfeld and Seger, 2005; Cagnol and Rivard, 2013; Caunt and Keyse, 2013). We used Western blot analysis to explore the potential for a loss of FMRP to affect the levels of DUSP protein. This was first tested in WT and KO tsA-201 cells exposed in culture medium to either vehicle alone or FMRP-N-tat (70 nM) for 7 h (Fig. 7B). These tests revealed a significant decrease in the level of DUSP6 in KO cells compared with that in WT cells. However, the lower levels of DUSP6 in KO cells were rescued by pretreating cells with 70 nM FMRP-N-tat for 7 h (Fig. 7B), a timeline that proved to overlap that required for FMRP-N-tat to rescue Cav3.1 modulation of Kv4.3 in *Fmr1* KO cells (compare Fig. 1F).

We then compared these results to the levels of DUSP detected in homogenates of the whole cerebellum from WT and *Fmr1* KO mice 24 h following tail vein injection of either

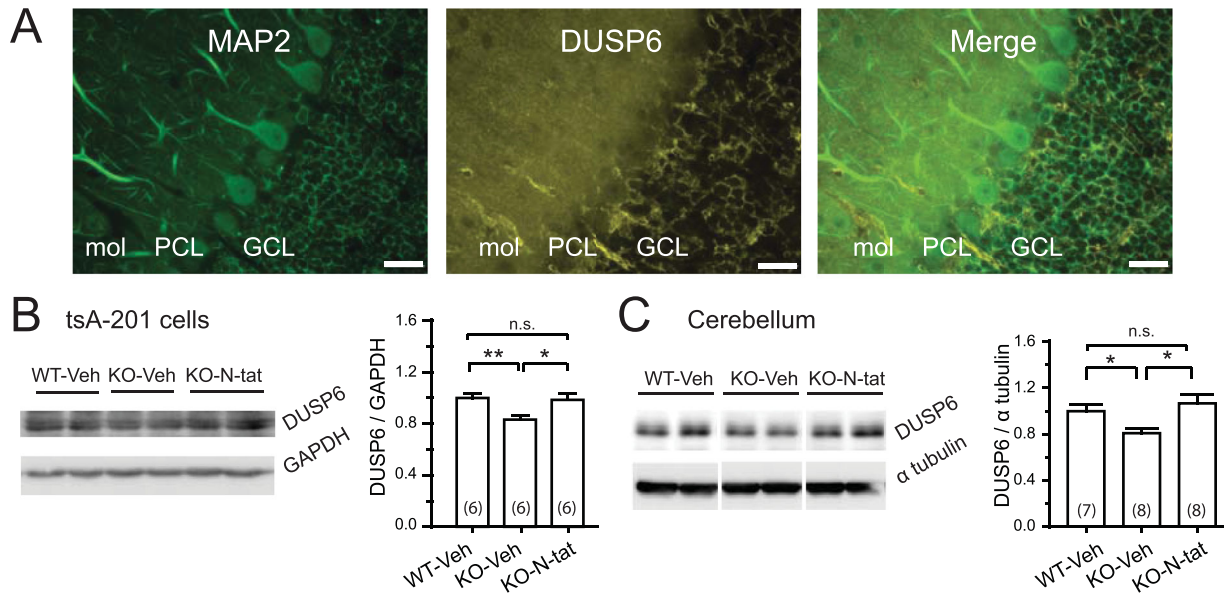


Figure 7. DUSP6 expression in cerebellum is disrupted in *Fmr1* KO cells but rescued by reintroducing FMRP-N-tat. **A**, Low-power immunofluorescence images for MAP-2 as a structural label and DUSP6 in tissue sections of P60 WT mouse lobule 9 cerebellum showing DUSP6 expression in granule cells. **B**, **C**, Two representative Western blots of the relative expression levels of DUSP6 in homogenates of *Fmr1* WT and KO tsA-201 cells (**B**) and P24–26 mouse cerebellar WT and *Fmr1* KO tissue (**C**). Protein levels are normalized to levels of GAPDH (**B**) and α -tubulin (**C**). DUSP6 levels are lower in tsA-201 *Fmr1* KO cells (**B**) and *Fmr1* KO cerebellum compared with WT (**C**). Direct application of 70 nM FMRP-N-tat in tsA-201 culture cell medium restores the level of DUSP6 (**B**), as found in *Fmr1* KO cerebellar tissue 24 h after tail vein injection of 1.0 mg/kg FMRP-N-tat (**C**). Average values are mean \pm SEM with sample sizes (*n*) indicated in bar plots. n.s., not significant; * $p < 0.05$; ** $p < 0.01$. Student's two-sample *t* test. Mol, molecular layer; PCL, Purkinje cell layer; GCL, granule cell layer. Scale bars (**A**), 50 μ m.

vehicle or FMRP-N-tat (Fig. 7C). In this case we found that the level of DUSP6 in the cerebellum was significantly reduced in *Fmr1* KO mice compared with that in WT mice (Fig. 7B). Yet once again, tail vein injection of *Fmr1* KO mice with 1 mg/kg FMRP-N-tat promoted a rescue of the level of DUSP6 in the cerebellum when tested 24 h later (Fig. 7C).

These data are important in identifying dual actions of FMRP-N-tat in reassociating with the Cav3-Kv4 complex at the plasma membrane to restore calcium-dependent regulation (Fig. 6) as well as restoring a disrupted level of DUSP (Fig. 7) that is critical to the function of the Cav3-Kv4 complex.

Discussion

Cav3 calcium channels form a nanodomain association with a Kv4-KChIP complex to confer calcium-dependent modulation of I_A that can influence signal processing (Vierra and Trimmer, 2022). Despite our knowledge of the functional outputs of the Cav3-Kv4 complex, the molecular mechanisms underlying calcium-dependent control of Kv4 channels had not been fully explored. The current study identified a critical role for FMRP in enabling a new Cav3-DUSP signaling pathway to regulate ERK-mediated phosphorylation in the complex. The physiological relevance of FMRP to Cav3-Kv4 function was further shown by the rescue of a hyperexcitable state and DUSP levels in cerebellar granule cells in the *Fmr1* KO mouse model for 24 h by in vivo administration of FMRP-N-tat.

FMRP as a member of the Cav3-Kv4-KChIP complex

An association between Kv4 potassium channels and KChIP proteins as a potential calcium-sensing element has long been recognized (An et al., 2000; Jerng et al., 2005; Pioletti et al., 2006; Wang et al., 2007), followed by recognition of Cav3 calcium channels as a component of the complex (Molineux et al., 2005). The role of FMRP as a critical element tightly associated with this

complex was identified through co-IP or FRET imaging. Thus, FMRP co-IPs with each of Cav3.1, Kv4.3, and KChIP3 (Fig. 2, Extended Data Fig. 2-1) and exhibits FRET with both Cav3.1 and Kv4.3 (Zhan et al., 2020). The FMRP-KChIP3 association proves to be unique in exhibiting a calcium-dependent loss of co-IP (i.e., dissociation; Fig. 2), a result not apparent for the co-IP between FMRP and either Cav3.1 or Kv4.3 (Extended Data Fig. 2-1). The current work using a *Fmr1* KO tsA-201 cell line provides evidence that the modulation of Kv4.3 also involves Cav3.1 calcium-dependent activation of DUSP to control the levels of pERK-mediated phosphorylation. It is interesting to note that several studies have been carried out on how the Cav3-Kv4 complex shapes the postsynaptic response of cerebellar stellate and granule cells (Molineux et al., 2005; Anderson et al., 2010a,b, 2013; Heath et al., 2014; Rizwan et al., 2016; Zhan et al., 2020). A retrospective analysis indicates that the new findings of a role for FMRP in the Cav3-Kv4 complex do not conflict in any way with results of these studies. Rather, FMRP proves to have been a hidden component that is central to the entire process by which Kv4 channels achieve calcium-dependent regulation.

Calcium-dependent control of Kv4 and I_A availability

Our available data supports a working model of actions that underlie calcium-dependent regulation of Kv4.3 for the combination of FMRP, Cav3.1, Kv4.3, and KChIP3 (Fig. 8). Under normal conditions, FMRP is associated with each of the protein subunits of the Cav3.1-Kv4.3-KChIP3 complex, with some resting level of phosphorylation of both Kv4.3 and FMRP at MAPK consensus sites that maintains a relatively low amplitude I_A (Fig. 8A). Membrane depolarization induces Cav3.1-mediated calcium entry that activates DUSP1/6 to dephosphorylate ERK. The decrease in pERK levels is then reflected in a reduction in phosphorylation of Kv4.3 along with an increase in phosphorylation of FMRP. Associated with calcium influx is a dissociation of FMRP-KChIP3 and a KChIP3-induced positive shift in Kv4.3

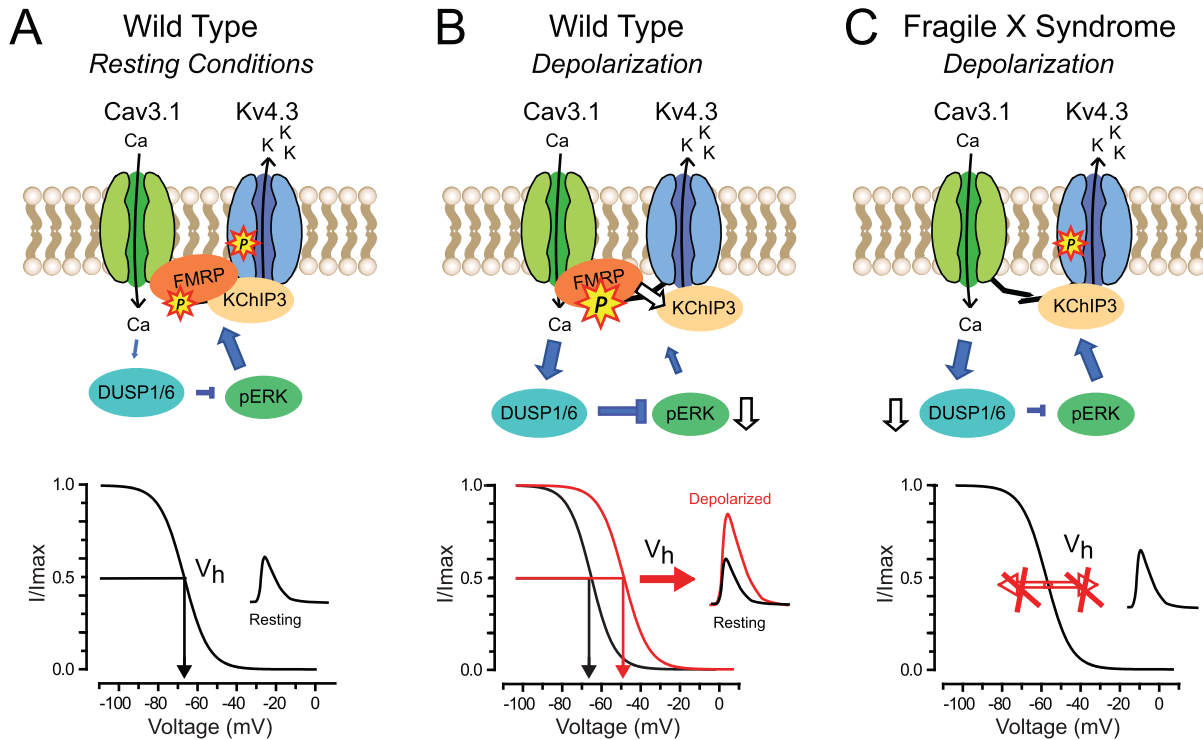


Figure 8. Model of FMRP regulation of calcium-dependent modulation of Kv4 channels via a DUSP-ERK pathway. Interactions shown are relevant to mouse cerebellar lobule 9 granule cells where Cav3.1, Kv4.3, KChIP3, and FMRP form a tight association at the plasma membrane. **A–C**, Shown are interactions found at rest and in response to depolarization in WT cells (**A**, **B**) and the effects of depolarization in the case of a loss of FMRP in FXS (**C**). **A**, Under resting conditions, a low Cav3.1 conductance provides little activation of DUSP1/6 that leads to an elevation of pERK. Both FMRP and Kv4.3 exhibit phosphorylation at MAPK consensus sequence sites, promoting a hyperpolarizing shift in Kv4.3 V_h (white arrow) that reduces IA amplitude. **B**, Upon membrane depolarization, Cav3.1 calcium conductance increases, activating DUSP1/6 to reduce levels of pERK and MAPK phosphorylation of Kv4.3 at a pSer site and an increase in phosphorylation at a pSer site on FMRP. Accompanying this is a reduction of the FMRP-KChIP3 association (white arrow) and a depolarizing shift in Kv4.3 V_h (red-filled arrow) that increases IA amplitude. **C**, In FXS a loss of FMRP from the complex and its interactions with KChIP3 prevents all calcium-dependent regulation of Kv4.3 V_h and IA amplitude (double arrows marked by X). In the *Fmr1* KO cerebellum, the level of DUSP6 is reduced but rescued along with the function of the Cav3-Kv4 complex upon reintroducing the FMRP(1-297) fragment as a tat-conjugated peptide.

V_h that increases I_A amplitude to reduce membrane excitability (Fig. 8B). The converse effect of a hyperpolarizing shift in Kv4.3 V_h can be revealed by reducing Cav3.1 calcium conductance, decreasing [Ca]_i, or by direct intracellular infusion of pERK. In the *Fmr1* KO mouse cerebellum, the level of DUSP6 is reduced, indicating a role for FMRP in regulating translation and expression of a phosphatase important to Cav3-Kv4 function (Fig. 8C). The lack of FMRP further removes the ability to phosphorylate FMRP and its dissociation from KChIP3, which together blocks all calcium-dependent regulation of Kv4.3 V_h and I_A amplitude (Fig. 8C). Thus, it appears that FMRP is required for KChIP3 to carry out its role of producing calcium-dependent shifts in Kv4.3 V_h . This model helps account for the sensitivity of Kv4 channels to fluctuations of calcium conductance that provides a bidirectional control over subunit phosphorylation by ERK and IA availability.

Distinct pathways to modulate I_A and membrane excitability

It is well established that mGluR/NMDAR activation provides a source of calcium influx to trigger the interplay between ERK, PP2A, and S6K1 to modify the phosphorylation state of FMRP (Bagni and Greenough, 2005; D'Incal et al., 2022). Bursts of mossy fiber input to stimulate mGluR/NMDARs on granule cells were also shown to activate ERK that reduced I_A to increase the spike output as part of mossy fiber LTP (Rizwan et al., 2016). Yet the current work reveals a new Cav3.1 channel-activated signaling pathway that does not involve PP2A and instead deactivates ERK to increase I_A .

The data thus suggest the existence of two pathways that can separately employ ERK to modulate I_A availability. One is intrinsic to the cell in being triggered by Cav3.1 calcium influx to activate DUSP and reduce pERK and phosphorylation of Kv4.3. This Cav3-dependent process also depends on a dynamic change in an FMRP-KChIP3 association, with the net effect of inducing a depolarizing shift of Kv4.3 V_h to increase I_A and reduce spike frequency. The second pathway requires an mGluR/NMDAR stimulus that activates ERK to induce a hyperpolarizing shift in Kv4 V_h to decrease I_A and promote a long-term increase in excitability in a manner that is also FMRP-dependent. At this time the exact means by which mGluR/NMDA activation results in a pERK-mediated increase in excitability is unknown but is expected to involve both pre- and postsynaptic mechanisms (Zhan et al., 2020). However, both the intrinsic and synaptically evoked process depend on calcium-dependent modulation of Kv4 V_h that in turn relies on FMRP.

Rescue of FMRP function in FXS

A number of strategies have been developed to reduce the symptoms of FXS through pharmacology (Yamasue et al., 2019), reactivating FMRP expression (Xie et al., 2016; Graef et al., 2019; Yrigollen and Davidson, 2019; Shah et al., 2023), or inducing FMRP expression through delivery of viral constructs (Hampson et al., 2019). It was recently found that reintroducing the N-terminus of FMRP as a tat conjugate peptide achieved rapid transport across the BBB, rescuing circuit functions and alleviating symptoms of *Fmr1* KO mice (Zhan et al., 2020).

The current work now shows that a loss of FMRP and its actions in the Cav3-Kv4 complex increases the intrinsic excitability of cerebellar granule cells to promote a hyperexcitable state of post-synaptic spike discharge. Tail vein injection of FMRP-N-tat fully rescued granule cell excitability in terms of postsynaptic spike properties and the level of DUSP even 24 h after tail vein injection. It is striking that FMRP-N-tat is able to restore the actions of FMRP both within an ion channel complex at the membrane while also modifying the expression level of a phosphatase that is key to calcium-dependent modulation of IA. It is important to note that the N-terminal region of FMRP has also been shown to restore GABAergic inhibition from basket cells to Purkinje cells in *Fmr1* KO mice (Yang et al., 2018). Conditional expression of FMRP in Purkinje cells of global *Fmr1* KO mice further restores Purkinje cell excitability (Stoodley et al., 2017; Gibson et al., 2023). The potential thus exists for FMRP fragments to exert therapeutic actions on several different parameters of cerebellar circuit dysfunction in FXS.

Cerebellar role in ASD in FXS

The behavioral and cognitive functions affected in FXS fall into the realm of ASD. The cerebellum is highly implicated given its established role in higher levels of cognition (D'Mello and Stoodley, 2015; Stoodley et al., 2017; Mapelli et al., 2022; Gibson et al., 2023). Indeed, a change in the output of cerebellar Purkinje cells in the right Crus I/II region has been shown to account for a range of ASD symptoms that include hypersensitivity to sensory stimuli (Tsai et al., 2012, 2018; D'Mello and Stoodley, 2015; Cupolillo et al., 2016; Peter et al., 2016; Stoodley et al., 2017; Sundberg et al., 2018; Gibson et al., 2023). A loss of FMRP has also been shown to alter the activity of granule (Zhan et al., 2020), Purkinje (Koekkoek et al., 2005; Gibson et al., 2023; Martín et al., 2023), and basket cells (Yang et al., 2018). Our work was conducted on granule cells in the vermis of lobule 9 in the posterior cerebellum, a region that has a role in processing multiple sensory inputs and exhibits functional connectivity with limbic structures (Sang et al., 2012; Markwalter et al., 2019). To our knowledge, a direct link between granule cell activity and ASD symptoms in FXS has not yet been defined as for Purkinje cells and ASD. Yet, a change in the intrinsic excitability of granule cells will alter signal processing at the first stage of mossy fiber input to the cerebellum that will affect cerebellar cortical activity and finally the output to neocortical regions that are predicted to contribute to ASD.

References

- Adams JP, Anderson AE, Varga AW, Dineley KT, Cook RG, Pfaffinger PJ, Sweatt JD (2000) The A-type potassium channel Kv4.2 is a substrate for the mitogen-activated protein kinase ERK. *J Neurochem* 75:2277–2287.
- An WF, et al. (2000) Modulation of A-type potassium channels by a family of calcium sensors. *Nature* 403:553–556.
- Anderson D, Mehaffey WH, Iftinca M, Rehak R, Engbers JD, Hameed S, Zamponi GW, Turner RW (2010a) Regulation of neuronal activity by Cav3-Kv4 channel signaling complexes. *Nat Neurosci* 13:333–337.
- Anderson D, Rehak R, Hameed S, Mehaffey WH, Zamponi GW, Turner RW (2010b) Regulation of the KV4.2 complex by CaV3.1 calcium channels. *Channels* 4:163–167.
- Anderson D, Engbers JD, Heath NC, Bartoletti TM, Mehaffey WH, Zamponi GW, Turner RW (2013) The Cav3-Kv4 complex acts as a calcium sensor to maintain inhibitory charge transfer during extracellular calcium fluctuations. *J Neurosci* 33:7811–7824.
- Asiminas A, et al. (2019) Sustained correction of associative learning deficits after brief, early treatment in a rat model of fragile X syndrome. *Sci Transl Med* 11:eaa0498.
- Bagni C, Greenough WT (2005) From mRNP trafficking to spine dysmorphogenesis: the roots of fragile X syndrome. *Nat Rev Neurosci* 6:376–387.
- Cagnol S, Rivard N (2013) Oncogenic KRAS and BRAF activation of the MEK/ERK signaling pathway promotes expression of dual-specificity phosphatase 4 (DUSP4/MKP2) resulting in nuclear ERK1/2 inhibition. *Oncogene* 32:564–576.
- Callsen B, Isbrandt D, Sauter K, Hartmann LS, Pongs O, Bähring R (2005) Contribution of N- and C-terminal Kv4.2 channel domains to KChIP interaction. *J Physiol* 568:397–412.
- Caunt CJ, Armstrong SP, Rivers CA, Norman MR, McArdle CA (2008) Spatiotemporal regulation of ERK2 by dual specificity phosphatases. *J Biol Chem* 283:26612–26623.
- Caunt CJ, Keyse SM (2013) Dual-specificity MAP kinase phosphatases (MKPs): shaping the outcome of MAP kinase signalling. *FEBS J* 280:489–504.
- Choi J, Park JH, Kwon OY, Kim S, Chung JH, Lim DS, Kim KS, Rhim H, Han YS (2005) T-type calcium channel trigger p21ras signaling pathway to ERK in Cav3.1-expressed HEK293 cells. *Brain Res* 1054:22–29.
- Contractor A, Klyachko VA, Portera-Cailliau C (2015) Altered neuronal and circuit excitability in fragile X syndrome. *Neuron* 87:699–715.
- Cupolillo D, Hoxha E, Faralli A, De Luca A, Rossi F, Tempia F, Carulli D (2016) Autistic-Like traits and cerebellar dysfunction in purkinje cell PTEN knock-out mice. *Neuropsychopharmacology* 41:1457–1466.
- Curia G, Gualtieri F, Bartolomeo R, Vezzali R, Biagini G (2013) Resilience to audiogenic seizures is associated with p-ERK1/2 dephosphorylation in the subiculum of *Fmr1* knockout mice. *Front Cell Neurosci* 7:1–13.
- D'Angelo E, De Zeeuw CI (2009) Timing and plasticity in the cerebellum: focus on the granular layer. *Trends Neurosci* 32:30–40.
- Deng P-Y, Klyachko VA (2021) Channelopathies in fragile X syndrome. *Nat Rev Neurosci* 22:275–289.
- D'Incal C, Broos J, Torfs T, Kooy RF, Vanden Berghe W (2022) Towards kinase inhibitor therapies for fragile X syndrome: tweaking twists in the autism spectrum kinase signaling network. *Cells* 11:1325, 1–45.
- D'Mello AM, Stoodley CJ (2015) Cerebellar-cerebellar circuits in autism spectrum disorder. *Front Neurosci* 9:1–18.
- Ferron L, Ruchon Y, Renaud J-F, Capuano V (2011) T-type Ca²⁺ signalling regulates aldosterone-induced CREB activation and cell death through PP2A activation in neonatal cardiomyocytes. *Cardiovasc Res* 90:105–112.
- Gall D, Roussel C, Susa I, D'Angelo E, Rossi P, Bearzatto B, Galas MC, Blum D, Schurmans S, Schiffmann SN (2003) Altered neuronal excitability in cerebellar granule cells of mice lacking calretinin. *J Neurosci* 23:9320–9327.
- Gallagher A, Hallahan B (2012) Fragile X-associated disorders: a clinical overview. *J Neurol* 259:401–413.
- Garrido JA, Ros E, D'Angelo E (2013) Spike timing regulation on the millisecond scale by distributed synaptic plasticity at the cerebellum input stage: a simulation study. *Front Comput Neurosci* 7:64.
- Gibson JM, Vazquez AH, Yamashiro K, Jakkamsetti V, Ren C, Lei K, Dentel B, Pascual JM, Tsai PT (2023) Cerebellar contribution to autism-relevant behaviors in fragile X syndrome models. *Cell Rep* 42:113533, 1–17.
- Giovannucci A, et al. (2017) Cerebellar granule cells acquire a widespread predictive feedback signal during motor learning. *Nat Neurosci* 20:727–734.
- Graef JD, et al. (2019) Partial FMRP expression is sufficient to normalize neuronal hyperactivity in fragile X neurons. *Eur J Neurosci* 51:2143–2157.
- Hahn K, Miranda M, Francis VA, Vendrell J, Zorzano A, Teleman AA (2010) PP2A regulatory subunit PP2A-B' counteracts S6 K phosphorylation. *Cell Metab* 11:438–444.
- Hampson DR, Hooper AWM, Niibori Y (2019) The application of adeno-associated viral vector gene therapy to the treatment of fragile X syndrome. *Brain Sci* 9:32, 1–15.
- Heath NC, Rizwan AP, Engbers JD, Anderson D, Zamponi GW, Turner RW (2014) The expression pattern of a Cav3-Kv4 complex differentially regulates spike output in cerebellar granule cells. *J Neurosci* 34:8800–8812.
- Jerng HH, Kunjilwar K, Pfaffinger PJ (2005) Multiprotein assembly of Kv4.2, KChIP3 and DPP10 produces ternary channel complexes with ISA-like properties. *J Physiol* 568:767–788.
- Kim SH, Markham JA, Weiler IJ, Greenough WT (2008) Aberrant early-phase ERK inactivation impedes neuronal function in fragile X syndrome. *Proc Natl Acad Sci U S A* 105:4429–4434.
- Koekkoek SK, et al. (2005) Deletion of FMR1 in Purkinje cells enhances parallel fiber LTD, enlarges spines, and attenuates cerebellar eyelid conditioning in fragile X syndrome. *Neuron* 47:339–352.

- Liu X, Kumar V, Tsai N-P, Auerbach BD (2021) Hyperexcitability and homeostasis in fragile X syndrome. *Front Mol Neurosci* 14:805929.
- Mapelli L, Soda T, D'Angelo E, Prestori F (2022) The cerebellar involvement in autism spectrum disorders: from the social brain to mouse models. *Int J Mol Sci* 23:3894, 1–34.
- Markwalter KH, Yang Y, Holy TE, Bonni A (2019) Sensorimotor coding of vermal granule neurons in the developing mammalian cerebellum. *J Neurosci* 39:6626–6643.
- Martín R, Suárez-Pinilla AS, García-Font N, Laguna-Luque ML, López-Ramos JC, Oset-Gasque MJ, Gruart A, Delgado-García JM, Torres M, Sánchez-Prieto J (2023) The activation of mGluR4 rescues parallel fiber synaptic transmission and LTP, motor learning and social behavior in a mouse model of fragile X syndrome. *Mol Autism* 14:1–21.
- Molina G, et al. (2009) Zebrafish chemical screening reveals an inhibitor of Dusp6 that expands cardiac cell lineages. *Nat Chem Biol* 5:680–687.
- Molineux ML, Fernandez FR, Mehaffey WH, Turner RW (2005) A-type and T-type currents interact to produce a novel spike latency-voltage relationship in cerebellar stellate cells. *J Neurosci* 25:10863–10873.
- Molineux ML, McRory JE, McKay BE, Hamid J, Mehaffey WH, Rehak R, Snutch TP, Zamponi GW, Turner RW (2006) Specific T-type calcium channel isoforms are associated with distinct burst phenotypes in deep cerebellar nuclear neurons. *Proc Natl Acad Sci U S A* 103:5555–5560.
- Murari K, Abushaibah A, Rho JM, Turner RW, Cheng N (2023) A clinically relevant selective ERK-pathway inhibitor reverses core deficits in a mouse model of autism. *EBioMedicine* 91:104565, 1–17.
- Narayanan U, Nalavadi V, Nakamoto M, Pallas DC, Ceman S, Bassell GJ, Warren ST (2007) FMRP phosphorylation reveals an immediate-early signaling pathway triggered by group I mGluR and mediated by PP2A. *J Neurosci* 27:14349–14357.
- Osterweil EK, Chuang SC, Chubykin AA, Sidorov M, Bianchi R, Wong RK, Bear MF (2013) Lovastatin corrects excess protein synthesis and prevents epileptogenesis in a mouse model of fragile X syndrome. *Neuron* 77:243–250.
- Peter S, et al. (2016) Dysfunctional cerebellar Purkinje cells contribute to autism-like behaviour in Shank2-deficient mice. *Nat Commun* 7:12627, 1–14.
- Pioletti M, Findeisen F, Hura GL, Minor DL Jr (2006) Three-dimensional structure of the KChIP1-Kv4.3 T1 complex reveals a cross-shaped octamer. *Nat Struct Mol Biol* 13:987–995.
- Rizwan AP, Zhan X, Zamponi GW, Turner RW (2016) Long-term potentiation at the mossy fiber-granule cell relay invokes postsynaptic second-messenger regulation of Kv4 channels. *J Neurosci* 36:11196–11207.
- Rubinfeld H, Seger R (2005) The ERK cascade: a prototype of MAPK signaling. *Mol Biotechnol* 31:151–174.
- Sang L, Qin W, Liu Y, Han W, Zhang Y, Jiang T, Yu C (2012) Resting-state functional connectivity of the vermal and hemispheric subregions of the cerebellum with both the cerebral cortical networks and subcortical structures. *Neuroimage* 61:1213–1225.
- Scannevin RH, et al. (2004) Two N-terminal domains of Kv4 K(+) channels regulate binding to and modulation by KChIP1. *Neuron* 41:587–598.
- Schrader LA, Anderson AE, Mayne A, Pfaffinger PJ, Sweatt JD (2002) PKA modulation of Kv4.2-encoded A-type potassium channels requires formation of a supramolecular complex. *J Neurosci* 22:10123–10133.
- Schrader LA, Birnbaum SG, Nadin BM, Ren Y, Bui D, Anderson AE, David Sweatt J (2006) ERK/MAPK regulates the Kv4.2 potassium channel by direct phosphorylation of the pore-forming subunit. *Am J Physiol Cell Physiol* 290:C852–C861.
- Sgritta M, Locatelli F, Soda T, Prestori F, D'Angelo EU (2017) Hebbian spike-timing dependent plasticity at the cerebellar input stage. *J Neurosci* 37:2809–2823.
- Shah S, Sharp KJ, Raju Ponny S, Lee J, Watts JK, Berry-Kravis E, Richter JD (2023) Antisense oligonucleotide rescue of CGG expansion-dependent FMR1 mis-splicing in fragile X syndrome restores FMRP. *Proc Natl Acad Sci U S A* 120:e2302534120, 1–11.
- Sharma A, Rahman G, Gorelik J, Bhargava A (2023) Voltage-gated T-type calcium channel modulation by kinases and phosphatases: the old ones, the new ones, and the missing ones. *Cells* 2:461, 1–123.
- Stoodley CJ, et al. (2017) Altered cerebellar connectivity in autism and cerebellar-mediated rescue of autism-related behaviors in mice. *Nat Neurosci* 20:1744–1751.
- Sundberg M, et al. (2018) Purkinje cells derived from TSC patients display hypoexcitability and synaptic deficits associated with reduced FMRP levels and reversed by rapamycin. *Mol Psychiatry* 23:2167–2183.
- Tsai PT, Hull C, Chu Y, Greene-Colozzi E, Sadowski AR, Leech JM, Steinberg J, Crawley JN, Regehr WG, Sahin M (2012) Autistic-like behaviour and cerebellar dysfunction in Purkinje cell Tsc1 mutant mice. *Nature* 488:647–651.
- Tsai PT, Rudolph S, Guo C, Ellegood J, Gibson JM, Schaeffer SM, Mogavero J, Lerch JP, Regehr W, Sahin M (2018) Sensitive periods for cerebellar-mediated autistic-like behaviors. *Cell Rep* 25:357–367.e4.
- Turner RW, Asmara H, Engbers JDT, Miclat J, Rizwan AP, Sahu G, Zamponi GW (2016) Assessing the role of IKCa channels in generating the sAHP of CA1 hippocampal pyramidal cells. *Channels* 10:313–319.
- Vierra NC, Trimmer JS (2022) Ion channel partnerships: odd and not-so-odd couples controlling neuronal ion channel function. *Int J Mol Sci* 23:1–19.
- Wagner MJ, Kim TH, Savall J, Schnitzer MJ, Luo L (2017) Cerebellar granule cells encode the expectation of reward. *Nature* 544:96–100.
- Wang H, et al. (2007) Structural basis for modulation of Kv4 K+ channels by auxiliary KChIP subunits. *Nat Neurosci* 10:32–39.
- Xie N, Gong H, Suhl JA, Chopra P, Wang T, Warren ST (2016) Reactivation of FMR1 by CRISPR/Cas9-mediated deletion of the expanded CGG-repeat of the fragile X chromosome. *PLoS One* 11:1–12.
- Yamasue H, Aran A, Berry-Kravis E (2019) Emerging pharmacological therapies in fragile X syndrome and autism. *Curr Opin Neurol* 32:635–640.
- Yang Y-M, et al. (2018) Identification of a molecular locus for normalizing dysregulated GABA release from interneurons in the fragile X brain. *Mol Psychiatry* 25:2017–2035.
- Yrigollen CM, Davidson BL (2019) CRISPR to the rescue: advances in gene editing for the FMR1 gene. *Brain Sci* 9:17, 1–14.
- Zhan X, Asmara H, Cheng N, Sahu G, Sanchez E, Zhang F-X, Zamponi GW, Rho JM, Turner RW (2020) FMRP(1-297)-tat restores ion channel and synaptic function in a model of fragile X syndrome. *Nat Commun* 11:2755, 1–16.